Manuscript No. 821

Revised Version

CRYOGENIC LIQUID HELIUM SLOSHING DYNAMICS DRIVEN BY SPACECRAFT ORBITAL ACCELERATIONS ASSOCIATED WITH SPINNING AND/OR SLEW MOTIONS

R. J. Hung and H. L. Pan

The University of Alabama in Huntsville

Huntsville, Alabama 35899, USA

Keywords: Superfluid Helium, Sloshing Dynamics, Microgravity, Spacecraft Spinning and Slew Motion, Gravity Gradient Acceleration

NASA-CR-197466

Abstract

The formulation of sloshing dynamics for partially filled liquid of cryogenic superfluid helium II in dewar containers driven by both the gravity gradient and jitter accelerations associated with spinning and/or slew motions in a microgravity environment are investigated. Both Gravity Probe-B (GP-B) and Advanced X-Ray Astrophysics Facility-Spectroscopy (AXAF-S) spacecrafts are given as realistic examples to elaborate the spacecraft operated with spinning and/or slew motions in which cryogenic superfluid helium II is used as a propellant . The jitter accelerations include slew motion, spinning motion, atmospheric drag on the spacecraft, spacecraft attitude motions arising from machinery vibrations, thruster firing, pointing control of spacecraft, crew motion, etc. The numerical computation of sloshing dynamics is carried out with the formulation of the non-inertia frame spacecraft bound coordinate, and solving time-dependent, three-dimensional formulations of partial differential equations subject to initial and boundary conditions. Examples are given to demonstrate how sloshing dynamics affected liquid-vapor interface oscillations of cryogenic superfluid helium II driven by orbital accelerations of spacecraft associated with spinning and/or slew motions.

I. Introduction

For the purpose to carry out scientific experiments, some experimental spacecraft use cryogenic cooling for observation instrumentation and telescope, superconducting sensors for gyro read-out and maintain very low temperature near absolute zero for mechanical stability. The approaches to both cooling and control involve the use of superfluid liquid helium II. To give examples, sloshing dynamics associated with spinning and/or slew motions are investigated. To cover the spacecraft spinning and/or slew motions, Gravity Probe-B (GP-B) and Advanced X-Ray Astrophysics Facility-Spectroscopy (AXAF-S) spacecrafts have been chosen as the examples in this study. Both the GP-B and the AXAF-S spacecrafts adopt the cooling and boil-off from the cryogenic liquid helium dewar as a cryogen and propellant to maintain the cooling of instrumentations, attitude control and drag-free operation of the spacecraft. The potential problems for cryogenic liquid in dewar container could be due to asymmetry in the unbalanced liquid-vapor distribution and to perturbations in the liquid-vapor interface caused by slosh wave excitation driven by pointing control, machinery vibration, etc.

For the cases of both the GP-B and the AXAF-S spacecrafts, cryogenic liquid helium II, at a temperature of 1.3 K, is used as the propellant. With its superconducting behavior, there is no temperature gradients in the liquid helium. In the absence of temperature gradient along the surface which drive Marangoni convection, the equilibrium shape of the liquid-vapor interface is governed by a balance of capillary, centrifugal and gravitational forces. Determination of liquid-vapor interface profiles based on computational experiments can uncover details of the flow which can not be easily visualized or measured experimentally in a microgravity environment.

The instability of the liquid-vapor interface surface can be induced by the presence of longitudinal and lateral accelerations. Slosh waves are, thus, excited which produces high and low frequency oscillations in the liquid propellant. The sources of the residual accelerations range from the effects of the Earth's gravity gradient and jitter accelerations which include, atmospheric drag on the spacecraft, vibration of compressor, spacecraft attitude motions arising from machinery vibrations, thruster firings, spacecraft slew motion, pointing control of spacecraft, crew motion, etc. Recent study[1] suggest that the high frequency accelerations may be unimportant in comparison to the residual motions caused by low frequency accelerations.

Time-dependent dynamical behavior of partially-filled rotating fluids in reduced gravity environments was simulated by numerically solving the Navier Stokes equations subject to the initial and the boundary conditions[2-5]. At the interface between the liquid and the gaseous fluids, both the kinematic surface boundary condition, and the interface stress conditions for components tangential and normal to the interface, were applied[6-10]. The initial conditions were adopted from the steady-state formulations developed by Hung et al[11-13]. Some of the steady-state formulations of interface shapes were compared with the available experiments carried out by Leslie[14] in a free-falling aircraft (KC-135). The experiments carried out by Mason et al[15] showed that the classical fluid mechanics theory is applicable for cryogenic liquid helium in large containers.

In the spacecraft orbit around the Earth, the direction of azimuth angle of Earth toward the location of the spacecraft mass center varies from 0° along the rolling axis of spacecraft to various directions in which three dimensional calculation shall be adopted.

As the spacecraft moves along the orbit, any fluid capable of motion relative to the spacecraft is subject to the acceleration that arises from the gravity gradients of the Earth[16-18]. The interaction between the particle mass of fluid and the spacecraft mass due to gravity gradient accelerations[17] are capable for the excitation of slosh waves and disturb the fluid system which induces the fluctuations of viscous stress and its moment exerted on the containers of the spacecraft fluid systems. In the meanwhile, the sources of residual acceleration of gravity jitter range from atmospheric drag on the spacecraft, background gravity, spacecraft attitude motions arising from machinery vibrations, spacecraft slew motion, thruster firings, crew motion, etc., are also capable for the excitation of slosh waves on the fluid containers.

It is critically important to understand the physical and dynamical behavior of liquid helium II in a rotating cylinder to effectively promote space-oriented missions associated with cryogenic systems.

At temperatures close to absolute zero, quantum effects begin to be of importance in the properties of fluids. At a temperature of 2.17°K, liquid helium has a λ-point (a second-order phase transition); at temperatures below this point liquid helium (helium II) has a number of remarkable properties, the most important of which is superfluidity. This is the property of being able to flow without viscosity in narrow capillaries or gaps.

The basis of the dynamics of helium II is the following fundamental result of microscopic theory. At temperatures other than zero, helium II behaves as if it were a mixture of two different liquids. One of these is a superfluid and moves with zero viscosity along a solid surface. The other is a normal viscous fluid. It is of great importance that no friction occurs between these two parts of the liquid in their relative motion, i.e., no momentum is transferred from one

to the other.

It should be emphasized that regarding the liquid as a mixture of normal and superfluid parts is no more than a convenient description of the phenomena which occur in a fluid where quantum effects are important. One of these motions is normal and has the same properties as the motion of an ordinary viscous fluid, but the other is the motion of a superfluid. The two motions occur without any transfer of momentum from one to another. We can, in a certain sense, speak of the superfluid and normal parts of the fluid, but this does not mean that the fluid can actually be separated into two such parts.

If fluid flow can separate helium II into the regions of the superfluid and the normal fluid, two temperatures zones are immediately created. A very low temperature zone is located at the zone of very high density concentration of the superfluid, while a high temperature (below 2.17° K) zone is located at the zone of very high density concentration of the normal fluid at the other end. The existence of a sharp temperature gradient at the interface between the superfluid and the normal fluid results in the creation of a great difference in chemical potential, which, in turn, induces a great reverse pressure gradient, creating the environment of isothermal fluid distribution everywhere throughout the cylinder and homogenous distribution of superfluid density concentration. This illustration of the possible separation of superfluid from normal fluid of helium II means that there is in reality, no way for anyone to achieve the separation of the superfluid from the normal fluid of helium II. In other words, in considering the dynamical behavior of helium II in a large rotating cylinder, a mixture of the superfluid and the normal fluid without separation of the two fluids is accounted for in the model computation. Density concentration of superfluid is a function of temperature, which is also true for the surface

tension and viscous coefficient for helium II[19-22]. In fact, the experiments carried out by Mason et al.[15] showed that the classical fluid mechanics theory is applicable for cryogenic liquid helium in a large container. In this study, the theory of viscous Newtonian fluids is employed with modification of transport coefficients adjusted by normal and superfluid density concentration which is a function of temperature.

II. Functions of Scientific Observation and Spacecraft Motions

Various scientific satellites operate on different orbits depending upon the scientific missions. We are particularly interested in the spacecraft operating with spinning and/or slew motions when it is operating around the Earth. Both the GP-B and the AXAF-S spacecrafts are sun synchronous Earth satellites orbiting at 650 km altitude directly over the poles and also operating with spinning and/or slew motions. The functions of scientific observation for both the GP-B and the AXAF-S spacecrafts and their motions are illustrated as follows:

(A) GP-B Spacecraft

The GP-B spacecraft is a relativity gyroscope experiment to test two extraordinary, undiversified predictions of Albert Einstein's general theory of relativity[23-25]. By using gyroscopes (ones with electrically supported spheres, spinning in a vacuum and others which utilize the spins of atomic nuclei, circulating sound waves, and even circulating laser beams), the GP-B measures two distinct space-time processes, <u>frame dragging</u> and the <u>geodetic effect</u>, which gradually changes its directions of spin. In these gyroscopes, the underlying principle is that rotating systems, free from disturbing forces, should remain pointing in the same direction in space.

In order to insure these extremely precise and accurate measurements and

gyroscope operations, near zero temperature is required for mechanical stability of the instrument, preservation of the lead bag magnetic shield, shielding the gyroscopes against nongravitation disturbances, and for reading their direction of spin. Near zero temperature cryogenic liquid helium II (1.3°K) has been chosen to serve this purpose[15-27].

To comprise these functions of scientific observation, GP-B stores its gyroscopes, telescope, probe mass and others in the center core of the dewar probe surrounded by the cryogenic helium II liquid. The dewar container of the GP-B is spinning with a rotating rate of 0.1 rpm during normal operation. As the telescope is constantly sighted on Rigel, gyro spin directions also pointing toward Rigel during the spacecraft moving around the polar orbit. The GP-B with its rotating dewar, there is no slew motion involved in the spacecraft motion.

(B) AXAF-S Spacecraft

The AXAF-S with its sister spacecraft AXAF-I (I for imaging) are two spacecrafts restructured from the original AXAF design to carry out astrophysical observation. Equipped with the (microcalorimeter) X-Ray Spectrometer (XRS), AXAF-S provides high-throughput, high-resolution, non-dispersive spectroscopy at the higher AXAF x-ray energies - including the astrophysically important iron-K spectral region (above 6.4 keV) - and also permits some spatially resolved high-resolution spectroscopy. AXAF-S comprises a foil-mirror (or possibly, a replication-optic) telescope (4.7-m focal length), with XRS in the focal plane. With the baseline optical system, the AXAF-S provides important, unique capabilities for high-throughput, high resolution (above 1 keV) spectroscopy of extended and point sources and for some spatially resolved high-resolution spectroscopy.

To comprise these functions of scientific observation, AXAF-S equipped with

foil-mirror telescope and XRS in the focal plane is capable to observe point and extended sources of active galactic nuclei, clusters of galaxies, supernova remnants, x-ray binaries, stellar flares, active regions of corona, etc., through spacecraft slew motion of pointing control. In other words, spacecraft slew motion without spinning with rotating axis is required for AXAF-S to perform its scientific mission.

III. Basic Characteristics of Gravity Gradient and Gravity Jitter Accelerations

Any fluid element inside the on-orbit spacecraft fluid system is subject to the acceleration that arises from the gravity gradient of the Earth[16-18]. Once the spacecraft orbit is fixed, the orbit period is determined and the basic structure of the gravity gradient acceleration also can be calculated. However, gravity gradient acceleration acting on each fluid element inside the on-orbit spacecraft fluid system is different dependent upon the distance of the location of the fluid element to the geometrical center of the spacecraft and its direction toward the location of the center of the Earth. This acceleration can only be calculated based on the non-inertia frame of spacecraft bound coordinate. Thus, the coordinate system shall be transformed from ordinary inertia frame coordinate to non-inertia coordinate.

(A) Orbit Motion of Spacecraft

Let us consider the cases of the GP-B and the AXAF-S spacecrafts, which are the Earth satellites orbiting at 650 km altitude directly over the poles, the orbit period, τ_o can be computed from following expression:

$$\tau_o = 2\pi \frac{R_c^{3/2}}{R_E g_o^{1/2}} \qquad (3\text{-}1)$$

where R_E denotes the radius of Earth (= 6373 km); R_c, the radius of the circular

orbit (= R_E + h = 7023 km); h, orbit altitude (= 650 km); and g_o, Earth gravity acceleration (= 9.81 $^m/s^2$). For the cases of both GP-B and AXAF-S spacecrafts, the orbit period τ_o = 97.6 min, and orbit rate n = $^{2\pi}/\tau_o$ = 1.07 x 10^{-3} $^{rad}/_s$.

As the spacecraft is orbiting around the Earth, the azimuth angle of the Earth, ψ_E, toward the location of the spacecraft geometric center varies with respect to time. At time t = 0, the rolling axis of the spacecraft is aligned with the radial direction of the Earth's center to the spacecraft mass center. Assuming the spacecraft rolling axis is linearly turning around 0° to 360° in the orbit period, τ_o, of the spacecraft when the spacecraft is orbiting around the Earth. This is particularly true for the case of the GP-B spacecraft. Without the spacecraft slew motion, the azimuth angle (ψ_{Eo}) can be defined as

$$\psi_{E_o} = \frac{2\pi}{\tau_o} t \qquad (3\text{-}2)$$

where τ_o is the spacecraft orbit period [defined in Equation (3-1)]; and t is the time measured from the instant when the direction of the spacecraft rolling axis is aligned with the radial direction of the spacecraft mass center to the center of the Earth.

(B) Slew Motion of Spacecraft

For the purpose to carry out wide-range observations, some scientific spacecraft requires slew motion with respect to the mass center of the spacecraft. This is particularly true for the case of the AXAF-S spacecraft. For the case of the spacecraft slew motion, azimuth angle, shown in Equation (3-2), shall be modified through the coordinate transformation of slew motion when the spacecraft is orbiting around the Earth.

Let us assume that the slew motion starts with the center located at the mass center of the spacecraft. Let us choose cartesian coordinate (x'', y'',

z'') with z''-axis along the axis of the dewar container (see Figure 1). At time t = 0, the radial vector $\hat{r}_c$ from the center of the spacecraft to the center of the Earth lies on the x''-z'' plane of the cartesian coordinate chosen (see Figure 1). The azimuth angle ψ_E is defined as the angle between the radial vector $\hat{r}_c$ and the z"-axis. Rotation matrices for spinning and/or slew motions along the x"-, y"- and z"-axes can be expressed as

$$\begin{bmatrix} 1 & 0 & 0 \\ 0 & \cos\omega_x t & \sin\omega_x t \\ 0 & -\sin\omega_x t & \cos\omega_x t \end{bmatrix}, \begin{bmatrix} \cos\omega_y t & 0 & -\sin\omega_y t \\ 0 & 1 & 0 \\ \sin\omega_y t & 0 & \cos\omega_y t \end{bmatrix}, \begin{bmatrix} \cos\omega_z t & \sin\omega_z t & 0 \\ -\sin\omega_z t & \cos\omega_z t & 0 \\ 0 & 0 & 1 \end{bmatrix}$$

respectively. Here, ω_x, ω_y and ω_z denote angular velocity of slew and/or spinning motions along the x"-, y"- and z"-axes, respectively. Radial vector $\hat{r}_c$ in cartesian coordinate without slew and spinning motion is (see Figure 1)

$$\hat{f}_{co} = [\sin\psi_{Eo}, 0, -\cos\psi_{Eo}] \qquad (3\text{-}3)$$

With an execution of spinning motion along the z"-axis only, radial vector $\hat{r}_c$ becomes (see Figure 1)

$$\hat{f}_{c\text{-}z} = \begin{bmatrix} \cos\omega_z t & \sin\omega_z t & 0 \\ -\sin\omega_z t & \cos\omega_z t & 0 \\ 0 & 0 & 1 \end{bmatrix} \begin{bmatrix} \sin\psi_{Eo} \\ 0 \\ -\cos\psi_{Eo} \end{bmatrix}$$

$$= [\sin\psi_{Eo}\cos\omega_z t, -\sin\psi_{Eo}\sin\omega_z t, -\cos\psi_{Eo}] \qquad (3\text{-}4)$$

With an execution of slew motion along the y"-axis only, radial vector $\hat{r}_c$ becomes (see Figure 1)

$$\hat{f}_{c\text{-}y} = \begin{bmatrix} \cos\omega_y t & 0 & -\sin\omega_y t \\ 0 & 1 & 0 \\ \sin\omega_y t & 0 & \cos\omega_y t \end{bmatrix} \begin{bmatrix} \sin\psi_{Eo} \\ 0 \\ -\cos\psi_{Eo} \end{bmatrix}$$

$$= [\sin(\psi_{Eo}+\omega_y t), 0, -\cos(\psi_{Eo}+\omega_y t)] \qquad (3\text{-}5)$$

With an operation of slew motion along the x"-axis only, radial vector $\hat{r}_c$ becomes (see Figure 1)

$$\hat{r}_{c\text{-}x} = \begin{bmatrix} 1 & 0 & 0 \\ 0 & \cos\omega_x t & \sin\omega_x t \\ 0 & -\sin\omega_x t & \cos\omega_x t \end{bmatrix} \begin{bmatrix} \sin\psi_{Eo} \\ 0 \\ -\cos\psi_{Eo} \end{bmatrix}$$

$$= [\sin\psi_{Eo}, -\cos\psi_{Eo}\sin\omega_x t, -\cos\psi_{Eo}\cos\omega_x t] \qquad (3\text{-}6)$$

In other words, radial vector $\hat{r}_c$ will be modified from the mathematical expression shown in Equation (3-3) to (3-4), (3-5), and (3-6) for the slew and/or spinning motions along the z"-, y"-, and x"-axes alone, respectively. In particular, for the case of slew motion along the y"-axis, comparison between Equations (3-3) and (3-5), it shows that the azimuth angle will be modified as

$$\psi_E = \psi_{Eo} + \omega_y t \qquad (3\text{-}7)$$

For the successive operations of the spacecraft from spinning motion along the z"-axis, then slew motion along the y"-axis, and then slew motion along the x"-axis, radial vector $\hat{r}_c$ results

$$\hat{r}_{c\text{-}z,y,x} = \begin{bmatrix} 1 & 0 & 1 \\ 0 & \cos\omega_x t & \sin\omega_x t \\ 0 & -\sin\omega_x t & \cos\omega_x t \end{bmatrix} \begin{bmatrix} \cos\omega_y t & 0 & -\sin\omega_y t \\ 0 & 1 & 0 \\ \sin\omega_y t & 0 & \cos\omega_y t \end{bmatrix} \cdot$$

$$\cdot \begin{bmatrix} \cos\omega_z t & \sin\omega_z t & 0 \\ -\sin\omega_z t & \cos\omega_z & 0 \\ 0 & 0 & 1 \end{bmatrix} \begin{bmatrix} \sin\psi_{Eo} \\ 0 \\ -\cos\psi_{Eo} \end{bmatrix} \qquad (3\text{-}8)$$

In addition to the modification of the azimuth angle made by the spacecraft slew motion, accelerations are also induced to activate on the fluid mass in the dewar container. Accelerations acting on the fluid particle in the dewar induced

by the slew motion of the spacecraft with the coordinate fixed at the spacecraft center of the mass is as follows (see Figure 1):

$$\ddot{\vec{R}}_p = \vec{\omega} x (\vec{\omega} x \vec{R}_p) + \vec{\alpha} x \vec{R}_p + 2\vec{\omega} x \vec{v} \qquad (3\text{-}9)$$

where $\vec{R}_p$ denotes the position vector of the fluid particle in the dewar container relative to the body frame of the spacecraft; $\vec{\omega}$, angular velocity of the spacecraft body frame; $\vec{\alpha}$, angular acceleration of the spacecraft body frame; and $\vec{v}$, velocity of the fluid particle relative to the spacecraft body frame.

As we indicated earlier, let us assume that the slew motion starts with the center located at the spacecraft mass center, cartesian coordinate (x'', y'', z'') is chosen with origin located at the spacecraft mass center. Let us also assume that x''-z'' plane intersects the center of Earth and the spacecraft mass center. In other words, azimuth angle of Earth toward the spacecraft mass center lies in the x''-z'' plane. Slew motion is along both the x''- and y''-coordinates. Thus, $\vec{\omega}_s = (\omega_{sx}, \omega_{sy}, 0)$ and $\vec{\alpha}_s = (\alpha_{sx}, \alpha_{sy}, 0)$, $\ddot{\vec{R}}_p$ due to slew motion becomes

$$\ddot{\vec{R}}_{p,slew} = \begin{bmatrix} \ddot{R}_{x''} \\ \ddot{R}_{y''} \\ \ddot{R}_{z''} \end{bmatrix}_{slew} = \begin{bmatrix} \omega_{sy}(\omega_{sx}R_y - R_x\omega_{sy}) + \alpha_{sy}R_z + 2\omega_{sy}V_z \\ -\omega_{sx}(\omega_{sx}R_y - R_x\omega_{sy}) - \alpha_{sx}R_z - 2\omega_{sx}V_z \\ -R_z(\omega_{sx}^2 + \omega_{sy}^2) + (\alpha_{sx}R_y - \alpha_{sy}R_x) + 2(\omega_{sx}V_y - \omega_{sy}V_x) \end{bmatrix}_{slew} \qquad (3\text{-}10)$$

(C) Gravity Gradient Acceleration

The gravity gradient acceleration acting on the fluid mass of spacecraft can be shown as[17]

$$\hat{a}_{gg} = -n^2 [3 (\hat{r}_c \cdot \hat{d}) \hat{r}_c - \hat{d}] \qquad (3\text{-}11)$$

where $\hat{a}_{gg}$ denotes gravity gradient acceleration vector; $\hat{d}$, the vector (not unit vector) from the fluid element to the spacecraft mass center; $\hat{r}_c$, a unit vector

from the spacecraft mass center to the center of the Earth; and n, the orbit rate (see Figure 1).

It is assumed that the gravity gradient exerted on the mass center of the spacecraft orbiting around the Earth on its specified orbit is zero. In other words, all the gravity acceleration exerted on the spacecraft is nothing but the gravity gradient acceleration which is defined in Equation (3-11). In this study, we are interested in investigating how gravity gradient acceleration affects the dynamical behaviors of cryogenic fluid elements of helium.

For the convenience of mathematical calculation, let us describe all the parameters involved in Equation (3-11) in terms of cartesian coordinates. In order to match with the computer simulation, mathematical derivation are considered in the first quadrant. Figure 1 illustrates the geometrical relationship of the parameters shown in Equation (3-11).

Let us consider the fluid element of interests, m, located at (r, θ, z) in cylindrical coordinates and at (x, y, z) in cartesian coordinates. The origin of the two coordinate systems is located at the center bottom of the dewar tank. The slew and/or spinning motions, mentioned earlier, are executed at the spacecraft mass center with cartesian coordinate (x", y", z"). The geometry center or the spacecraft mass center is located at $z = L_c$. As $|\hat{d}|$ (not unit vector) is much smaller than the distance between the location of both the GP-B and AXAF-S spacecrafts mass centers to the center of the Earth, $\hat{r}_c$ (an unit vector) through the GP-B and the AXAF-S mass centers and $\hat{r}_c$ (an unit vector) through the fluid element, m, is basically the same. Assume that vector $\hat{r}_c$ lies in the x-z plane of the cartesian coordinate.

Radial vector $\hat{r}_c$ with the modification of slew and/or spinning motions along the x"-, y"-, z"-axes have been derived in Equations (3-3) to (3-8). Based

on the relationship between coordinates (x, y, z) and (x", y", z")

$$\begin{bmatrix} x \\ y \\ z-L_c \end{bmatrix} = \begin{bmatrix} 1 & 0 & 0 \\ 0 & 1 & 0 \\ 0 & 0 & 1 \end{bmatrix} \begin{bmatrix} x'' \\ y'' \\ z'' \end{bmatrix} \tag{3-12}$$

Vector $\hat{d}$ in (x, y, z) coordinate becomes

$$\hat{d} = [-r\cos\theta, -r\sin\theta, -(z-L_c)] \tag{3-13}$$

Substituting Equations (3-4) and (3-13) in (3-11), non-inertia frame expression of gravity gradient acceleration with spinning motion in z-axis becomes

$$\begin{bmatrix} a_{gg,x} \\ a_{gg,y} \\ a_{gg,z} \end{bmatrix}_{spinning\ in\ z\text{-}axis} = -n^2 \begin{bmatrix} 3[-r\sin\psi_{Eo}\cos(\theta+\omega_z t)+(z-L_c)\cos\psi_{Eo}]\sin\psi_{Eo}\cos\omega_z t + r\cos\theta \\ -3[-r\sin\psi_{Eo}\cos(\theta+\omega_z t)+(z-L_c)\cos\psi_{Eo}]\sin\psi_{Eo}\sin\omega_z t + r\sin\theta \\ -3[-r\sin\psi_{Eo}\cos(\theta+\omega_z t)+(z-L_c)\cos\psi_{Eo}]\cos\psi_{Eo} + (z-L_c) \end{bmatrix} \tag{3-14}$$

Substituting Equations (3-5) and (3-13) in (3-11), non-inertia frame expressions of gravity gradient acceleration with slew motion in y-axis becomes

$$\begin{bmatrix} a_{gg,x} \\ a_{gg,y} \\ a_{gg,z} \end{bmatrix}_{slew\ in\ y\text{-}axis} = -n^2 \begin{bmatrix} 3[-r\sin\psi\cos\theta+\cos\psi(z-L_c)]\sin\psi + r\cos\theta \\ r\sin\theta \\ -3[-r\sin\psi\cos\theta+\cos\psi(z-L_c)]\cos\psi + (z-L_c) \end{bmatrix} \tag{3-15}$$

where $\psi_E = \psi_{Eo} + \omega_y t$.

Substituting Equations (3-6) and (3-13) in (3-11), non-inertia frame expressions of gravity gradient acceleration with slew motion in x-axis becomes

$$\begin{bmatrix} a_{gg,x} \\ a_{gg,y} \\ a_{gg,z} \end{bmatrix}_{slew\ in\ x\text{-}axis} = -n^2 \begin{bmatrix} 3(-r\cos\theta\sin\psi_{Eo}+\cos\psi_{Eo}[r\sin\omega_x t\sin\theta+\cos\omega_x t(z-L_c)])\sin\psi_{Eo}+r\cos\theta \\ -3(-r\cos\theta\sin\psi_{Eo}+\cos\psi_{Eo})]\sin\omega_x t\sin\theta+\cos\omega_x t(z-L_c)])\cos\psi_{Eo}\sin\omega_x t+r\sin\theta \\ -3(-r\cos\theta\sin\psi_{Eo}+\cos\psi_{Eo}[r\sin\omega_x t\sin\theta+\cos\omega_x t(z-L_c)])\cos\psi_{Eo}\cos\omega_x t+(z-L_c) \end{bmatrix} \tag{3-16}$$

The relationship for the coordinate transformation from cartesian to cylindrical coordinates for any vector $\hat{F}$ (such as velocity or force vectors) in non-inertia frame of spacecraft bound coordinate can be shown as

$$\begin{bmatrix} F_r \\ F_\theta \\ F_z \end{bmatrix} = \begin{bmatrix} \cos\theta & \sin\theta & 0 \\ -\sin\theta & \cos\theta & 0 \\ 0 & 0 & 1 \end{bmatrix} \begin{bmatrix} F_x \\ F_y \\ F_z \end{bmatrix} \tag{3-17}$$

Thus, the gravity gradient acceleration located at (r, θ, z) can be computed from that located at (x, y, z), shown in Equations (3-14) to (3-16), from the following relation:

$$\hat{a}_{gg} = \begin{bmatrix} a_{gg,r} \\ a_{gg,\theta} \\ a_{gg,z} \end{bmatrix} = \begin{bmatrix} \cos\theta & \sin\theta & 0 \\ -\sin\theta & \cos\theta & 0 \\ 0 & 0 & 1 \end{bmatrix} \begin{bmatrix} a_{gg,x} \\ a_{gg,y} \\ a_{gg,z} \end{bmatrix} \tag{3-18}$$

(D) Jitter Accelerations

In addition to gravity gradient acceleration acting on the fluid element of on-orbit spacecraft fluid systems, there is another acceleration of gravity jitter also exerted forces on the fluid systems. The sources of residual acceleration of gravity jitter range from slew motion of spacecraft, atmospheric drag on the spacecraft, background gravity, spacecraft attitude motions arising from machinery vibrations, thruster firings, crew motion, etc., are also capable for the excitation of slosh waves in spacecraft fluid systems[1-10].

Among all of the varieties of jitter accelerations listed, accelerations induced by slew motion of the spacecraft dominate the forces activated on the spacecraft fluid systems. Two coordinate systems (cylindrical and cartesian) chosen in this study are (r, θ, z) with corresponding velocity components (u_r, u_θ, u_z) for cylindrical, and (x, y, z) with corresponding velocity components (u_x, u_y, u_z) for cartesian coordinates. The origin of these two coordinates are located at the central bottom of the dewar tank, as shown in Figure 1. The spacecraft center of mass, is located at (x_c, y_c, z_c) = (0, 0, L_c). The relationships of the force between cartesian and cylindrical coordinates are

$$\begin{bmatrix} \ddot{R}_x \\ \ddot{R}_y \\ \ddot{R}_z \end{bmatrix}_{slew} = \begin{bmatrix} F_x \\ F_y \\ F_z \end{bmatrix}_{slew} = \begin{bmatrix} \cos\theta & \sin\theta & 0 \\ -\sin\theta & 0 & 0 \\ 0 & 0 & 1 \end{bmatrix}^{-1} \begin{bmatrix} F_r \\ F_\theta \\ F_z \end{bmatrix}_{slew} \qquad (3\text{-}19)$$

A detailed expression of $[\ddot{R}_x, \ddot{R}_y, \ddot{R}_z]_{slew}$ are shown in Equation (3-10) of this paper. Jitter acceleration is a summation of acceleration induced by slew motion and others, such as atmospheric drag on the spacecraft, spacecraft attitude motions arising from machinery vibration, thruster firing, crew motion, etc. Thus, jitter acceleration can be expressed as

$$\hat{a}_{gj} = \begin{bmatrix} a_{gj,r} \\ a_{gj,\theta} \\ a_{gj,z} \end{bmatrix}_{slew} + \begin{bmatrix} a_{gj,r} \\ a_{gj,\theta} \\ a_{gj,z} \end{bmatrix}_{others} = -\begin{bmatrix} F_r \\ F_\theta \\ F_z \end{bmatrix}_{slew} - \begin{bmatrix} F_r \\ F_\theta \\ F_z \end{bmatrix}_{others} \{ 1 + \frac{1}{2}\sin(2\pi f t) \}$$

$$= -\begin{bmatrix} \cos\theta & \sin\theta & 0 \\ -\sin\theta & \cos\theta & 0 \\ 0 & 0 & 1 \end{bmatrix} \begin{bmatrix} F_x \\ F_y \\ F_z \end{bmatrix}_{slew} - \begin{bmatrix} F_r \\ F_\theta \\ F_z \end{bmatrix}_{others} \{ 1 + \frac{1}{2}\sin(2\pi f t) \} \qquad (3\text{-}20)$$

where f is the jitter frequency (Hz) imposed on the fluid systems of the spacecraft.

For the case of the GP-B spacecraft, there is no jitter acceleration associated with slew motion, i.e.,

$$\hat{a}_{gj} = -\begin{bmatrix} F_r \\ F_\theta \\ F_z \end{bmatrix}_{others} [1 + \frac{1}{2}\sin(2\pi f t)] = g \begin{bmatrix} \sin\psi_g \cos(\theta + \omega_z t) \\ -\sin\psi_g \sin(\theta + \omega_z t) \\ -\cos\psi_g \end{bmatrix} [1 + \frac{1}{2}\sin(2\pi f t)] \qquad (3\text{-}21)$$

IV. Mathematical Model of Sloshing Dynamics Driven by Orbital Accelerations Associated With Spinning and/or Slew Motions

Dynamical behavior of fluid elements inside the on-orbit spacecraft fluid systems are strongly modified by the gravity gradient acceleration associated with slew motion. In order to accommodate the impact of gravity gradient acceleration, in particular, on the on-orbit fluid motion, one has to consider

non-inertia frame of the spacecraft bound coordinate rather than adopting inertia frame coordinate used in ordinary fluid mechanics formulation.

Consider a closed circular cylinder of radius, a, with height, L, which is partially filled with cryogenic liquid helium, and the rest of the ullage is filed with a helium vapor. Density and viscosity of liquid helium and helium vapor are ρ_L, μ_L, ρ_v, and μ_v, respectively. Let us use the cylindrical coordinates (r, θ, z), with corresponding velocity components (u, v, w), and corresponding components of gravity gradient and jitter accelerations associated with slew motion are ($a_{gg,r}$, $a_{gg,\theta}$, $a_{gg,z}$), and ($a_{gj,r}$, $a_{gj,\theta}$, $a_{gj,z}$), respectively. The typical governing equations of continuity and full Navier-Stokes equations in non-inertia frame cylindrical coordinates are used in this study.

Detailed descriptions of the computational algorithm applicable to cryogenic fluid management under microgravity are also given in our earlier studies[6-10]. In this paper, a full-scale GP-B and AXAF spacecraft propellant dewar tanks with a radius of 68 cm and a height of 145 cm will be used in the numerical simulation. The propellant tank is 80% filled with cryogenic liquid helium for GP-B dewar and is 70% filled with cryogenic liquid helium for AXAF-S dewar while the rest of the ullage is filled with helium vapor. The temperature of cryogenic helium is 1.3 K. In this study the following data were used: liquid helium density = 0.145 g/cm^3, helium vapor density = 0.00147 g/cm^3, fluid pressure = 1.66 x 10^3 dyne/cm^2, surface tension coefficient at the interface between liquid helium and helium vapor = 0.346 dyne/cm, liquid helium viscosity coefficient = 1.12 x 10^{-4} cm^2/s; and contact angle = 5°. The initial profiles of the liquid-vapor interface for the rotating dewar are determined from computations based on algorithms developed for the steady state formulation of microgravity fluid management[11-13].

A staggered grid for the velocity components is used in this computer program. The method was developed by Harlow and Welch[26] for their MAC (marker-and-cell) method of studying fluid flows along a free surface. The finite difference method employed in this numerical study was the "Hybrid Scheme" developed by Spalding[27]. The formulation for this method is valid for any arbitrary interface location between the grid points and is not limited to middle point interfaces[28]. An algorithm for a semi-implicit method[29] was used as the procedure for modeling the flow field. The time step is determined automatically based on the size of the grid points and the velocity of flow fields. A detailed description of the computational algorithm applicable to microgravity fluid management is illustrated in our earlier studies[6-10]. Figures 2(A) and 2(B) show the distribution of grid points for the dewar tank with probe for GP-B dewar container in the radial-axial plane and radial-circumferential plane, respectively, in cylindrical coordinates. Figures 3(A) and 3(B) show the similar distribution of grid points for the dewar tank for the AXAF-S spacecraft in the radial-axial plane and radial-circumferential plane, respectively, in cylindrical coordinates.

V. Spacecraft Sloshing Dynamics Associated With Spinning and/or Slew Motions

By using the mathematical formulations illustrated in the previous sections, one can numerically simulate spacecraft sloshing dynamics associated with spinning and/or slew motions depending upon the specific scientific missions assigned to the spacecraft. Examples are given to illustrate sloshing dynamics associated with spinning motion for GP-B spacecraft, and sloshing dynamics associated with slew motion for the AXAF-S spacecraft.

(A) Sloshing Dynamics Associated With Spinning Motion for GP-B Spacecraft

As we described earlier, the dewar container of the GP-B is spinning with

a rotating rate of 0.1 rpm during its normal operation. Non-inertia frame fundamental equations, subject to initial and boundary conditions, shall be considered in our computation. As for gravity gradient acceleration, non-inertia frame expressions of Equations (3-14) and (3-18) for spinning motion in the z-axis shall be adopted. For gravity jitter acceleration, formulation shown in Equation (3-21) shall be used. In this equation, g denotes background equivalent gravity accelerations due to atmospheric drag on the spacecraft, spacecraft attitude motions arising from machinery vibrations, thruster firing, etc.

In this example, Figure 4 shows the time variation for gravity gradient acceleration for a turn-around periods of 1200 s with container rotating speed (ω_z) of 1.0 rpm for component along the (x, y, z) directions acted on the fluid mass located at (r, θ, z) = (60 cm, $\pi/4$, 40 cm). Figure 4 shows that the magnitude of gravity gradient acceleration is on the order of 10^{-7} g_o (= 981 cm/s^2). Figure 5 shows the time variation for gravity jitter accelerations for a turn-around period of 1200 s with a container rotating speed (ω_z) of 0.1 rpm and a jitter frequency (f) of 0.1 Hz for components along the (x, y, z) directions acted on the fluid mass everywhere in the container. Two ranges of background gravity, 10^{-6} and 10^{-8} g_o for gravity jitter accelerations which correspond to the magnitude of accelerations higher and lower, respectively, than that of the gravity gradient acceleration acted on the fluid system of the spacecraft are given in this example.

The equilibrium shape of the liquid-vapor interface for a rotating dewar under a residual gravity environment below 10^{-6} g_o and rotating speed of 0.1 rpm is very much alike and is a doughnut configuration with a near circular kidney-shape cross-section based on the computation of the numerical algorithm developed in our earlier studies[11-13]. Figure 6(A) shows the initial profile of the liquid-

vapor interface in the r-z plane at θ = 0° and 180°; Figure 6(B) shows the initial profile of the liquid-vapor interface in the r-z plane at θ = 90° and 270°; Figure 6(C) shows the initial profile of the liquid-vapor interface in the r-θ plane at height z = 108 cm; and Figure 6(D) shows the initial profile of three-dimensional liquid-vapor interface.

Sloshing dynamics of the GP-B spacecraft driven by the combined effects of gravity gradient and 10^{-8} g_o background jitter acceleration associated with spinning motion in the z-axis have been studied. In this case, the combined forces are dominated by the gravity gradient acceleration.

Figure 7 shows the time sequence evolution of the three-dimensional dynamical behavior of the interface oscillations driven by these combined accelerations. For the convenience of comparison, figures of liquid-vapor interface profiles with the same values of the time sequences chosen throughout the study of the GP-B sloshing dynamics are at time t = 191, 354, 380, 431, 503, 603, 825, 980, 995, 1050, 1080 and 1200 seconds. It clearly shows that there are a series of asymmetric oscillations excited fluctuations along the surface of sloshing dynamics governed liquid-vapor interface driven by asymmetric gravity-gradient-dominated acceleration associated with spinning motion in the z-axis.

The evolution of the capillary effect governed sloshing dynamics of interface oscillations at various cross-sections driven by gravity gradient-dominated acceleration associated with spinning motion in the z-axis are also examined. Figures 8 shows the time sequence of the sloshing dynamics governed liquid-vapor interface profiles, driven by the same gravity gradient-dominated acceleration as that shown in Figure 7, in the vertical r-z plane at θ = 0° and 180°. It indicates that the doughnut shape bubble (helium vapor) configurations change from axial symmetric to asymmetric profiles as ψ_E varies from 0° to 360°.

Sloshing dynamics of the GP-B spacecraft driven by the combined effects of gravity gradient and 10^{-6} g_o background jitter acceleration associated with spinning motion have also been studied. In this case, the combined forces are dominated by the jitter acceleration.

Figure 9 shows the time sequence evolution of the three-dimensional dynamical behavior of the sloshing dynamics governed interface oscillations driven by gravity jitter-dominated acceleration of 0.1 Hz low jitter frequency. It clearly shows that there are a series of asymmetric oscillations excited fluctuations along the surface of liquid-vapor interface driven by asymmetric gravity jitter-dominated acceleration.

The evolution of sloshing dynamics governed interface oscillations at various cross-sections driven by the same frequency of gravity jitter-dominated acceleration are also examined. Figures 10 shows the time sequence of the liquid-vapor interface profiles, driven by the same frequency of gravity jitter-dominated acceleration as that shown in Figure 9, in the vertical r-z plane at θ = 0° and 180°.

(B) Sloshing Dynamics Associated With Slew Motion for AXAF-S spacecraft

As we indicated earlier, AXAF-S spacecraft is capable to observe point and extended source of active galactic nuclei, clusters of galaxies, supernova remnants, x-ray binaries, etc., through spacecraft slew motion of pointing control. Assume that slew motion is along the y"-axis (see Figure 1), gravity gradient acceleration can be computed from the non-inertia frame expressions of Equations (3-15) and (3-18). It is assumed that the slew motion operates for the range of 90° in 10 minutes.

In this example, spacecraft sloshing dynamics driven by gravity gradient acceleration associated with slew motion in the y"-axis, shown in Figure 1, have

been investigated. As the orbital period of AXAF-S spacecraft is 97.6 min and period of slew motion in the y"-axis is 600 s, the component of gravity gradient acceleration along the (x, y, z) directions acted on the fluid mass located at $(r, \theta, z) = (12\ cm, \pi/2, 3\ cm)$ is shown in Figure 11. This figure shows that the magnitude of gravity gradient acceleration is on the order of $10^{-7}\ g_o$ for AXAF-S dewar on its operation orbit. The distance from the spacecraft mass center to the bottom of the dewar, L_c, shown in Figure 1, is 257.8 cm.

The equilibrium shape of the liquid-vapor interface dewar tank with 70% liquid-filled level under a residual gravity environment of $10^{-7}\ g_o$, as that shown in Figure 11, is a sphere. Figure 12(A) shows the initial profile of the liquid-vapor interface in the r-z plane at $\theta = 0°$ and 180°; Figure 12(B) shows the initial profile of liquid-vapor interface in the r-z plane at $\theta = 90°$ and 270°; Figure 12(C) shows the initial profile of the liquid-vapor interface in the r-θ plane at height z = 95.9 cm; and Figure 12(D) shows the initial profile of the three-dimensional liquid-vapor interface.

Sloshing dynamics of the AXAF-S spacecraft driven by the gravity gradient acceleration associated with slew motion in the y"-axis, shown in Figure 1, have been investigated. Figure 13 shows the time sequence evolution of the three-dimensional dynamical behavior of the interface oscillations driven by the gravity gradient acceleration associated with slew motion in the y"-axis. For the convenience of comparison, figures of the liquid-vapor interface profiles with the same values of the time sequences chosen throughout the study of the AXAF-S sloshing dynamics are at time t = 334, 392, 431, 456, 487, 524, 554, 588, 600, 695, 784 and 800 s. It clearly show that there are a series of asymmetric oscillations excited fluctuations along the surface of sloshing dynamics governed liquid-vapor interface driven by asymmetric gravity gradient acceleration

associated with slew motion in the y"-axis.

The evolution of the capillary effect governed sloshing dynamics of interface oscillations at various cross-sections driven by gravity gradient acceleration associated with slew motion in the y"-axis (see Figure 1) are also examined. Figure 14 shows the time sequence of the sloshing dynamics governed liquid-vapor interface profiles, driven by the same gravity gradient acceleration as that shown in Figure 13, in the vertical r-z plane at θ = 0° and 180°. It indicates that the spherical-shaped bubble (helium vapor) change from axial symmetric to asymmetric profiles during the course of slew motion.

VI. Discussion and Conclusion

With different scientific missions, some experimental spacecrafts have to operate with various spinning and/or slew motions for the purpose to perform its scientific experiments. In this study, both the GP-B and the AXAF-S spacecrafts have been given as the examples to show spacecrafts operated with spinning and/or slew motions. The instability of the liquid-vapor interface surface of the superfluid systems can be induced by the presence of gravity gradient and jitter accelerations associated with spinning and/or slew motions of the spacecraft. These instabilities originated from sloshing dynamics can cause various problems of spacecraft control systems. Sometimes, these sloshing dynamics problems can even deteriorate the quality of the normal operation of the spacecraft. It is vitally important to understand fully the characteristics of the spacecraft sloshing dynamics before one can assure the high quality operation of scientific spacecraft.

In this study, the formulation of sloshing dynamics for partially filled liquid in the dewar container driven by both the gravity gradient and jitter accelerations associated with spinning and/or slew motions are investigated. Two

examples of the numerical simulation for sloshing dynamics driven by orbital accelerations, one with the GP-B for spinning motion and the other with the AXAF-S for slew motion, have been carried out. These examples demonstrate how great the degrees of sloshing dynamics for imbalance profiles have been developed by the effects of orbital accelerations associated with spinning and/or slew motions. This study can provide a useful tool for the development of effective control techniques to assure the high quality operation of the spacecraft to achieve the final goal of scientific missions.

Acknowledgement

The authors appreciate the support received from the National Aeronautics and Space Administration through the NASA Grants NAG8-129 and NAG8-938, and also NASA contracts NAS8-38609/Delivery Order NO. 96. They would like to express their gratitude to Richard A. Potter of NASA/Marshall Space Flight Center for the stimulating discussions during the course of the present study.

References

1. Kamotani, Y., Prasad, A., Ostrach, S., AIAA Journal, 19, 511 (1981).
2. Hung, R. J., and Shyu, K. L., Microgravity Quarterly, 1(2), 81, (1991).
3. Hung, R. J., and Shyu, K. L., Acta Astronautica, 25, 709 (1991).
4. Hung, R. J., and Shyu, K. L., Journal of Spacecraft and Rockets, 29, 279, (1992).
5. Hung, R. J., and Shyu, K. L., Acta Astronautica, 26, 425, (1992).
6. Hung, R. J., and Shyu, K. L., Journal of Propulsion and Power, 8, 987, (1992).
7. Hung, R. J., Lee, C. C., and Leslie, F. W., Journal of Propulsion and Power, 7, 556, (1991).
8. Hung, R. J., Lee, C. C., and Leslie, F. W., Journal of Guidance, Control and Dynamics, 15, 817, (1992).
9. Hung, R. J., Lee, C. C., and Leslie, F. W., Journal of Fluids and Structures, 6, 493, (1992).
10. Hung, R. J., Lee, C. C., and Leslie, F. W., Transaction of the Japan Society for Aeronautical and Space Sciences, 35, 187, (1993).
11. Hung, R. J., Tsao, Y. D., Hong, B. B., and Leslie, F. W., International Journal for Microgravity Research and Applications, 11, 81, (1989).
12. Hung, R. J., Tsao, Y. D., Hong, B. B., and Leslie, F. W., Acta Astronautica, 19, 411, (1989).
13. Hung, R. J., Tsao, Y. D., Hong, B. B., and Leslie, F. W., Journal of Spacecraft and Rockets, 26, 167, (1989).
14. Leslie, F. W., Journal of Fluid Mechanics, 161, 269, (1985).
15. Mason, P., Collins, D., Petrac, D., Yang, L., Edeskuty, F., Schuch, A., and Williamson, K., Proceedings 7th International Cryogenic Engineering

Conferences, Surrey, England, Science and Technology Press, (1978).

16. Avduyevsky V. S. (editor), Scientific Foundations of Space Manufacturing, MIR, Moscow, USSR (1984).

17. Forward, R. L., Physical Review, Series D, 26, 735, (1982).

18. Misner; C. W., Thorne, K. S., and Wheeler, J. A., Gravitation, W. H. Freeman Co., San Francisco, CA, 1279, (1973).

19. Wilks, J., The Properties of Liquid and Solid Helium, Clarendon Press, Oxford, U.K., (1967).

20. Hoare, F. E., Jackson, L. C., and Kurti, N., Experimental Cryogenics; Liquid Helium II, Butterworths, London, U.K. (1961).

21. Hung, R. J., Proceedings of National Science Council, Series (A), 14, 289 (1990).

22. Hung, R. J., and Lee, C. C., Proceed. National Science Council (A), 16, 339, (1992).

23. Weinberg, S., Gravitation and Cosmology - Principles and Applications of General Relativity, 657, John Wiley and Sons, New York, (1972).

24. Hung, R. J., and Leslie, F. W., Journal of Spacecraft and Rockets, 25, 70, (1988).

25. Landau, L. D., and Lifshitz, Fluid Mechanics, Pergamon Press, London, 656, (1959).

26. Harlow, F. H., and Welch, F. E., Physics of Fluids, 8, 2182, (1965).

27. Spalding, D. B.,International Journal of Numerical Methods in Engineering, 4, 551, (1972).

28. Patanker, S. V., and Spalding, S. D., International Journal of Heat Mass Transfer, 15, 1787, (1972).

29. Patanker, S. V., Numerical Heat Transfer and Fluid Flow, Hemisphere-McGraw-

Hill, New York, NY, 197, (1980).

ON ORBIT COORDINATE SYSTEM

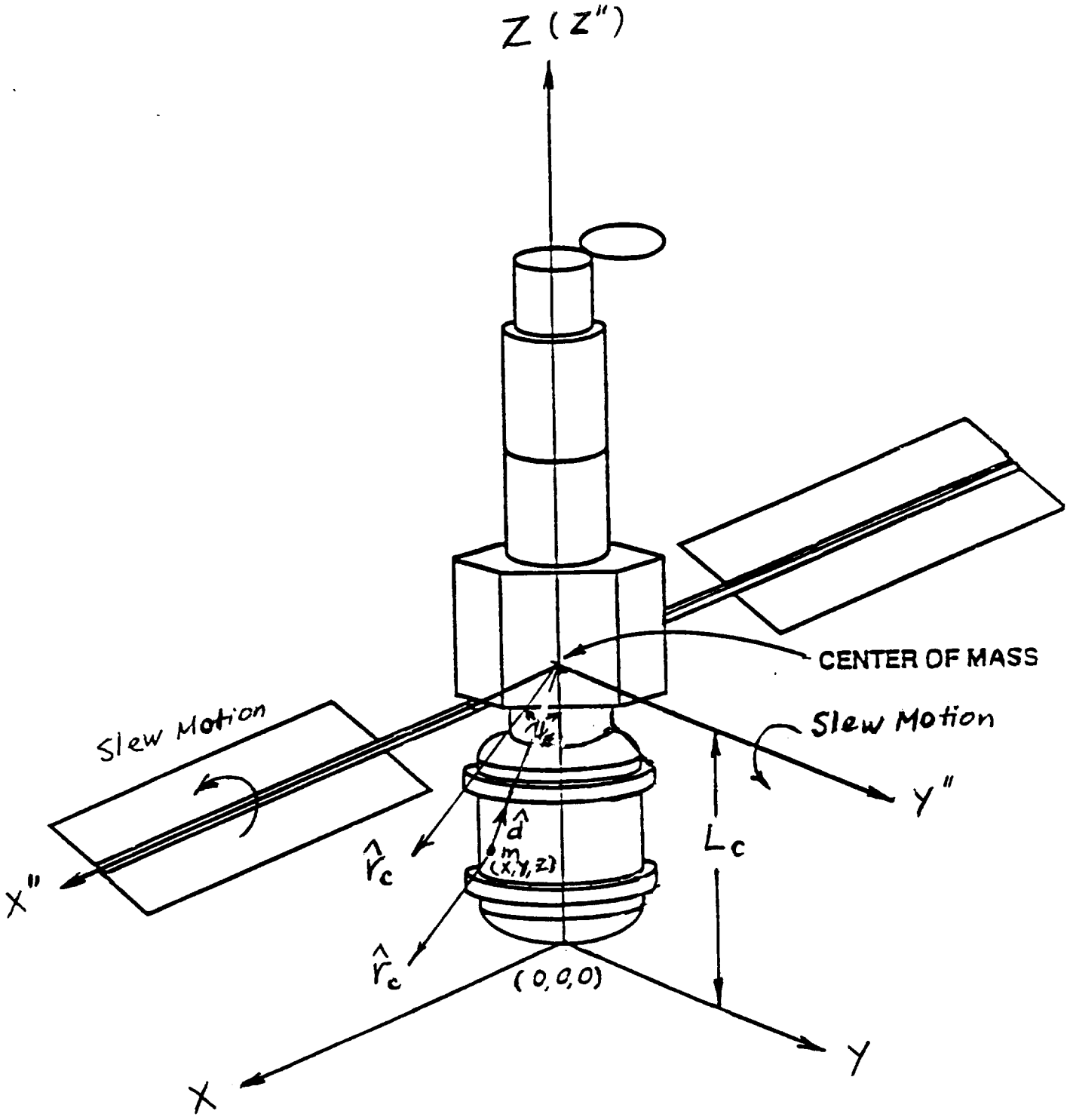

Figure 1

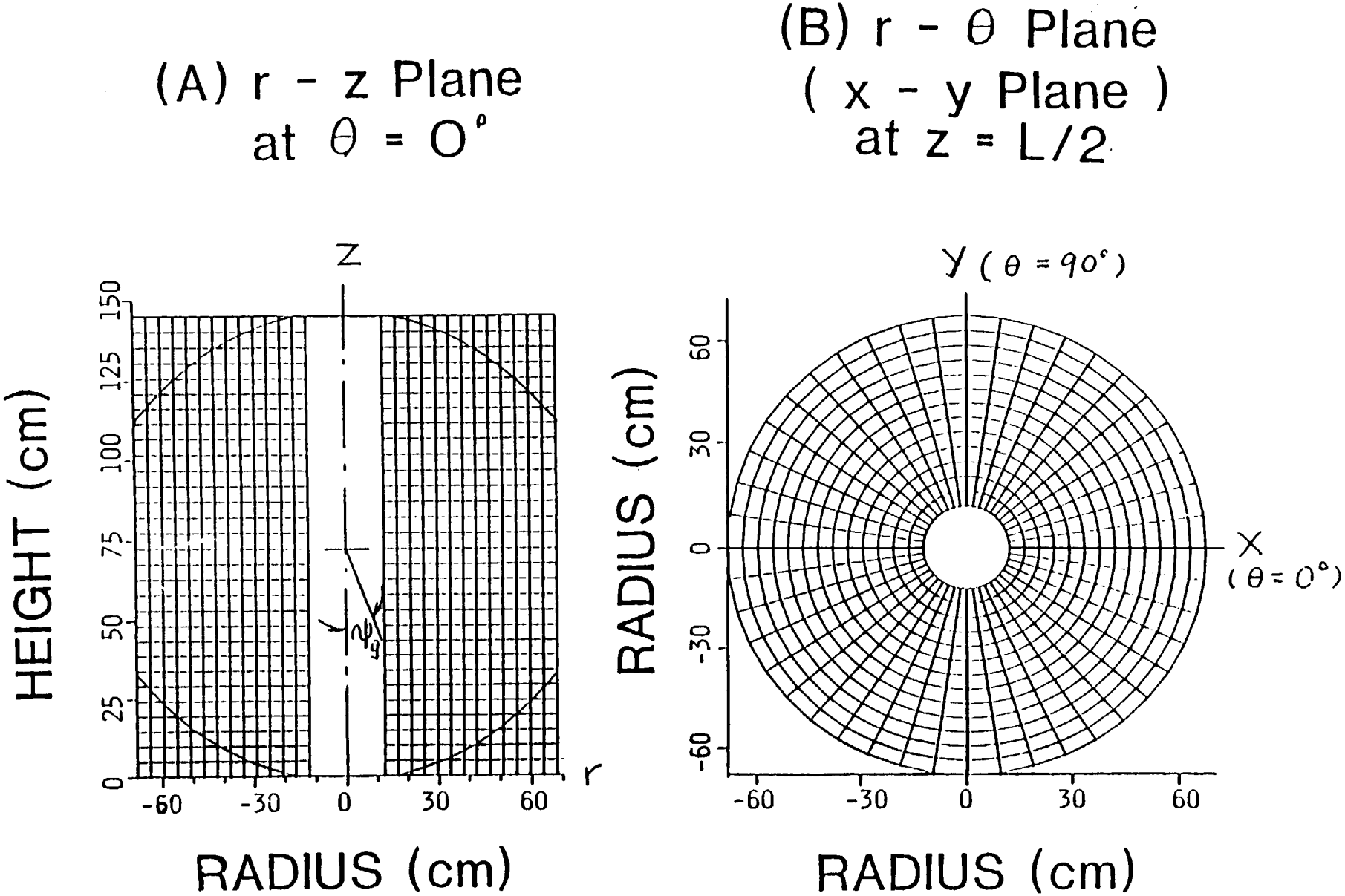
(A) r - z Plane
at θ = O°
(B) r - θ Plane
(x - y Plane)
at z = L/2
Z
HEIGHT (cm)
0
25
50
75
100
125
150
-60
-30
0
30
60
r
RADIUS (cm)
Y (θ = 90°)
RADIUS (cm)
60
30
0
-30
-60
X
(θ = 0°)
-60
-30
0
30
60
RADIUS (cm)

Fig. 2

(A) r - z Plane
at θ = O°

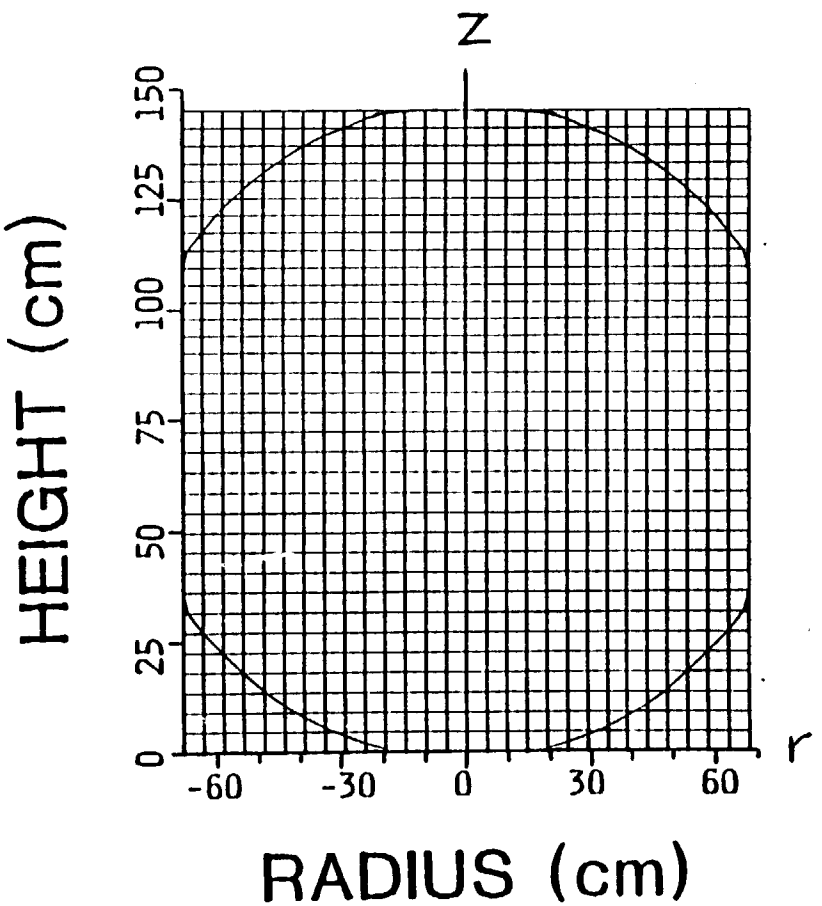

(B) r - θ Plane
(x - y Plane)
at z = L/2

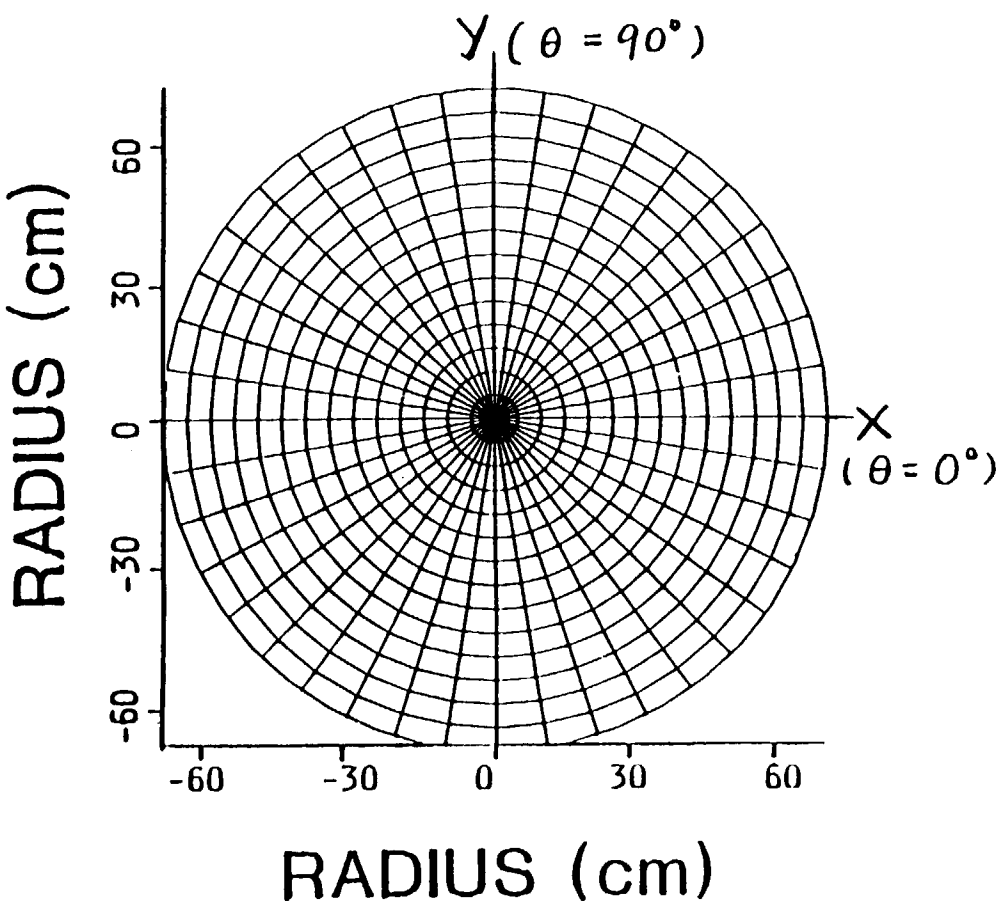

Fig. 3

Time Variation of Gravity Gradient Acceleration Acting on the GP-B Spacecraft Dewar Fluid Mass Located at

(r, θ, z)

$= (60\ \text{cm}, \pi/4, 40\ \text{cm})$

$\omega = 0.1$ rpm

$\tau = 1200$ s

$g_0 = 9.81\ \text{m/s}^2$

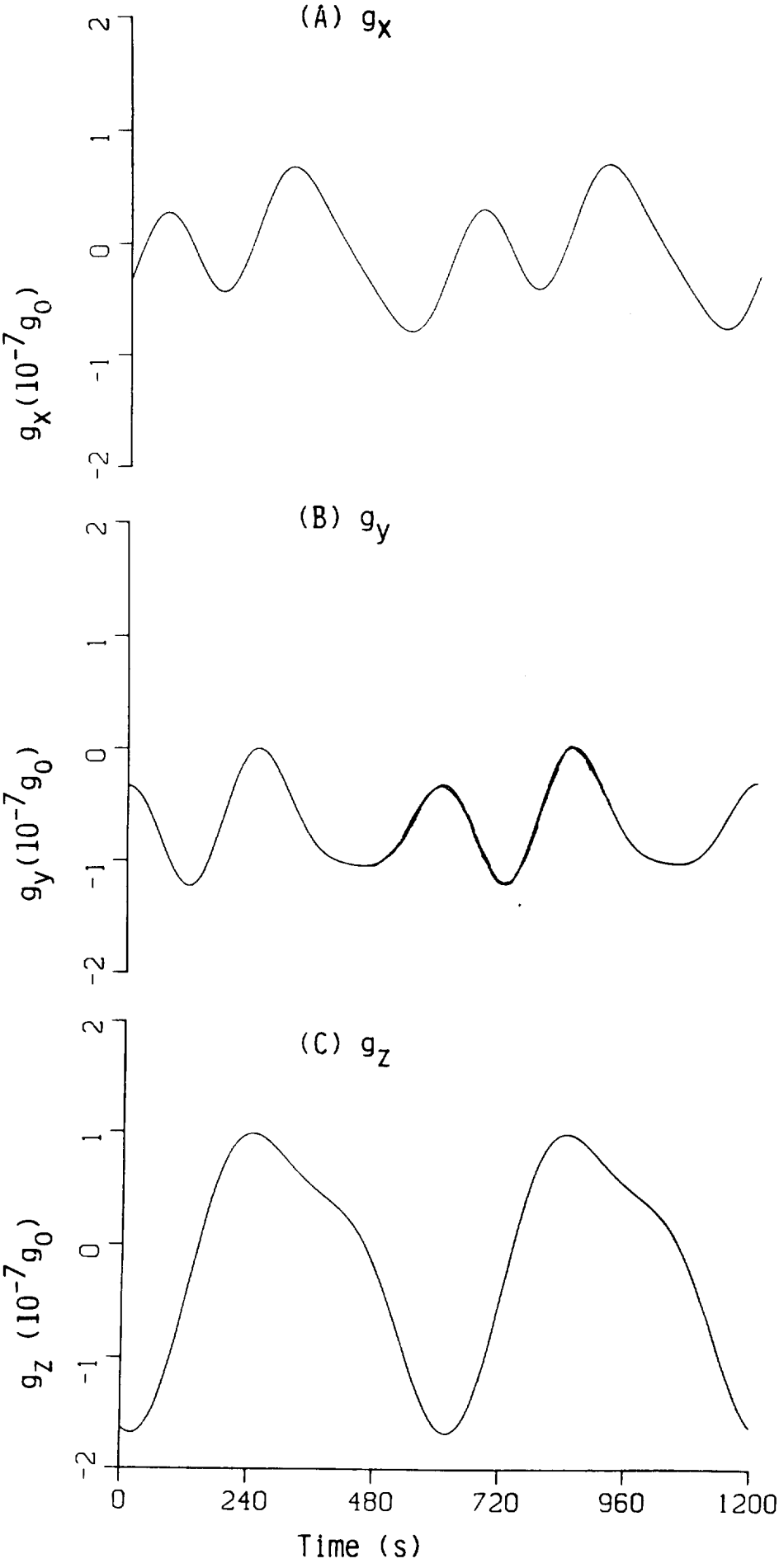

Fig. 4

Time Variation Of
Gravity Jitter
Acceleration Acting
on Spacecraft
Fluid System

$$g_B = \begin{bmatrix} 10^{-6} \\ 10^{-8} \end{bmatrix} g_0$$

ω = 0.1 rpm

f = 0.1 Hz

τ = 1200 s

g_0 = 9.81 m/s^2

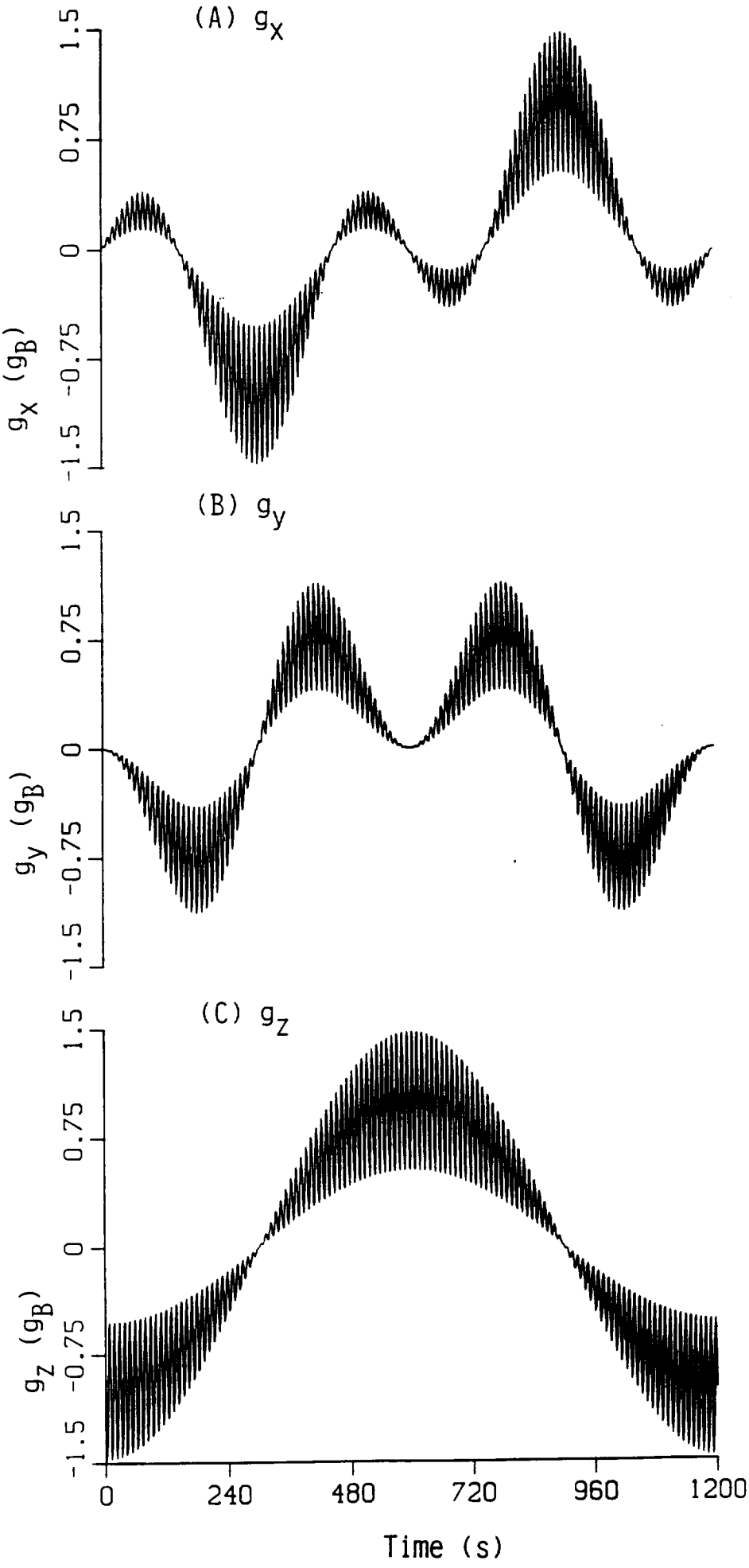

Fig.5

INITIAL PROFILES OF LIQUID HELIUM AND VAPOR INTERFACE

Rotating Dewar Under the Effect of Gravity Jitter

$g = 10^{-7} g_0$, $\omega = 0.1$ rpm, $\psi_{\xi} = 0^{\circ}$, $f = 0.1$ Hz

(A) r-z plane at $\theta = 0^{\circ}$ and 180°

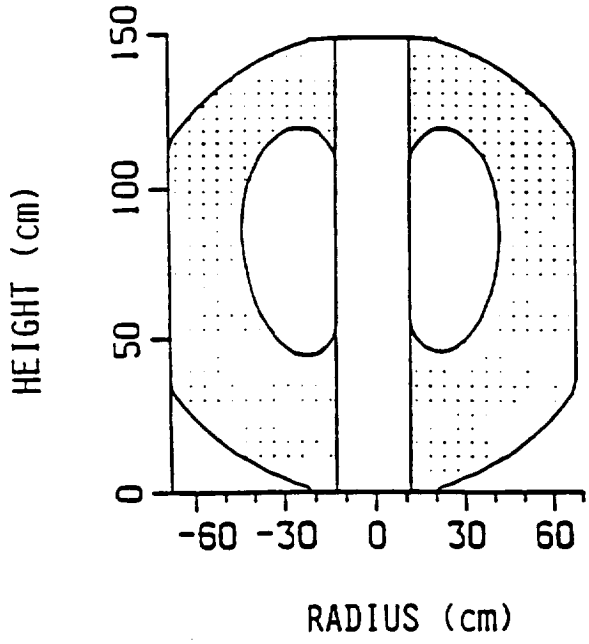

(B) r-z plane at $\theta = 90^{\circ}$ and 270°

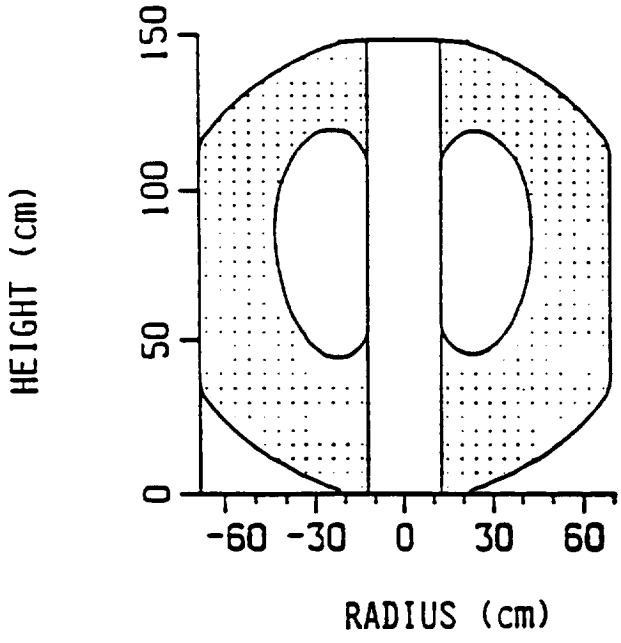

(C) r-θ plane at z = 108cm

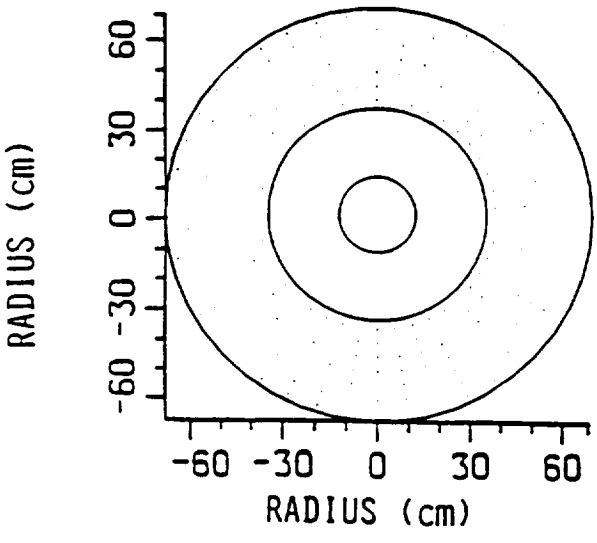

(D) Three-Dimensional Profiles

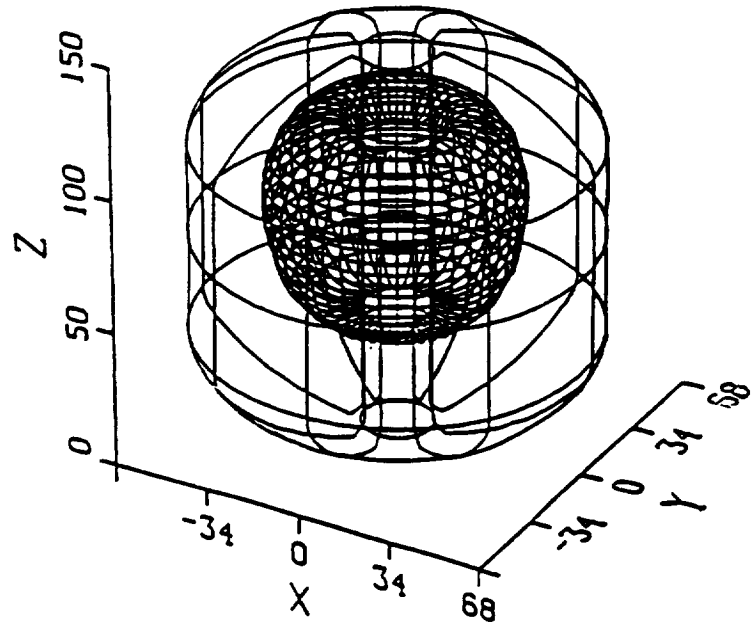

Fig. 6

THREE DIMENSIONAL LIQUID AND VAPOR INTERFACE

The Effect of Gravity Jitter and Gravity Gradient: $g = 10^{-8} g_0$

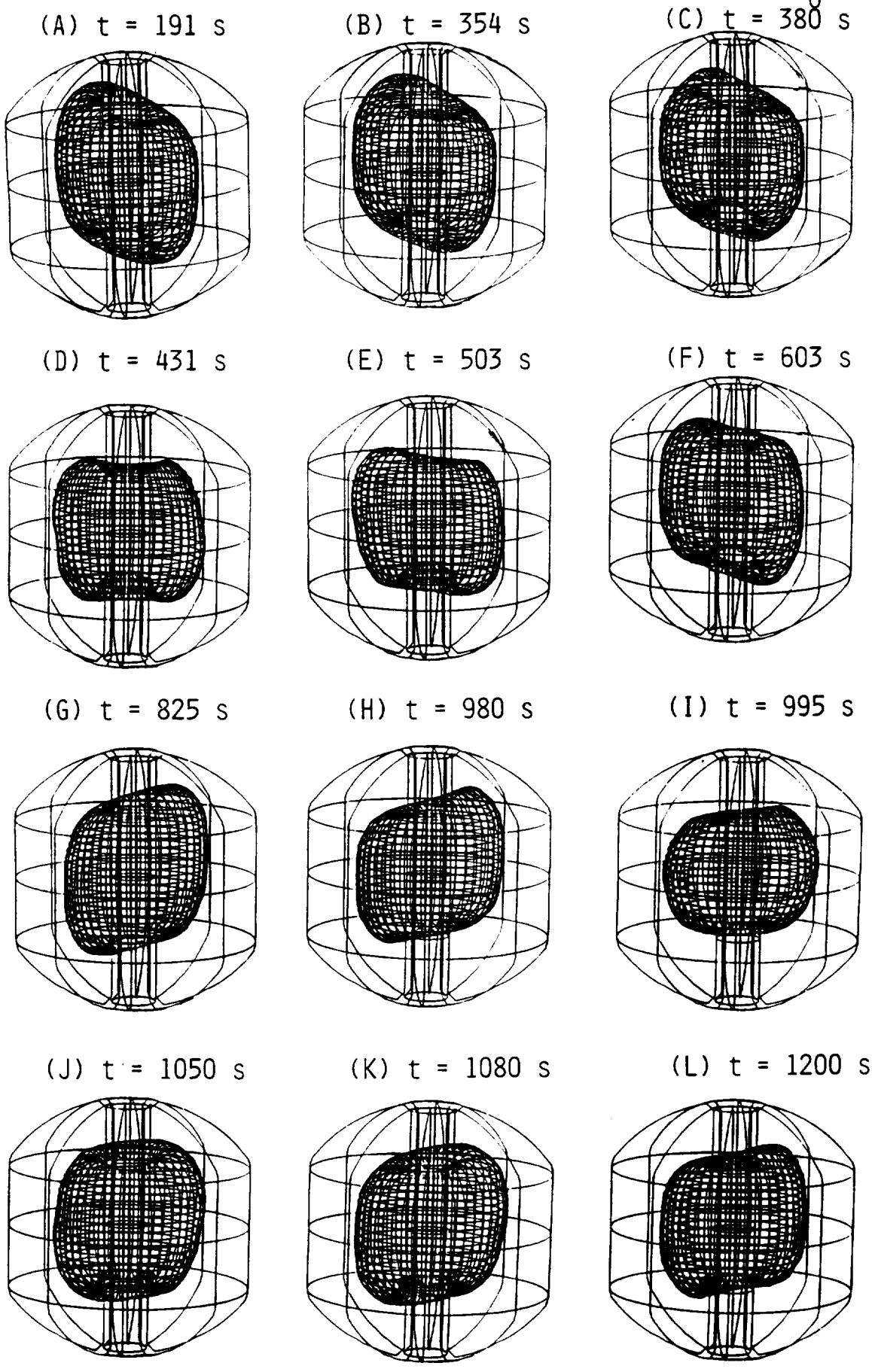

Fig. 7

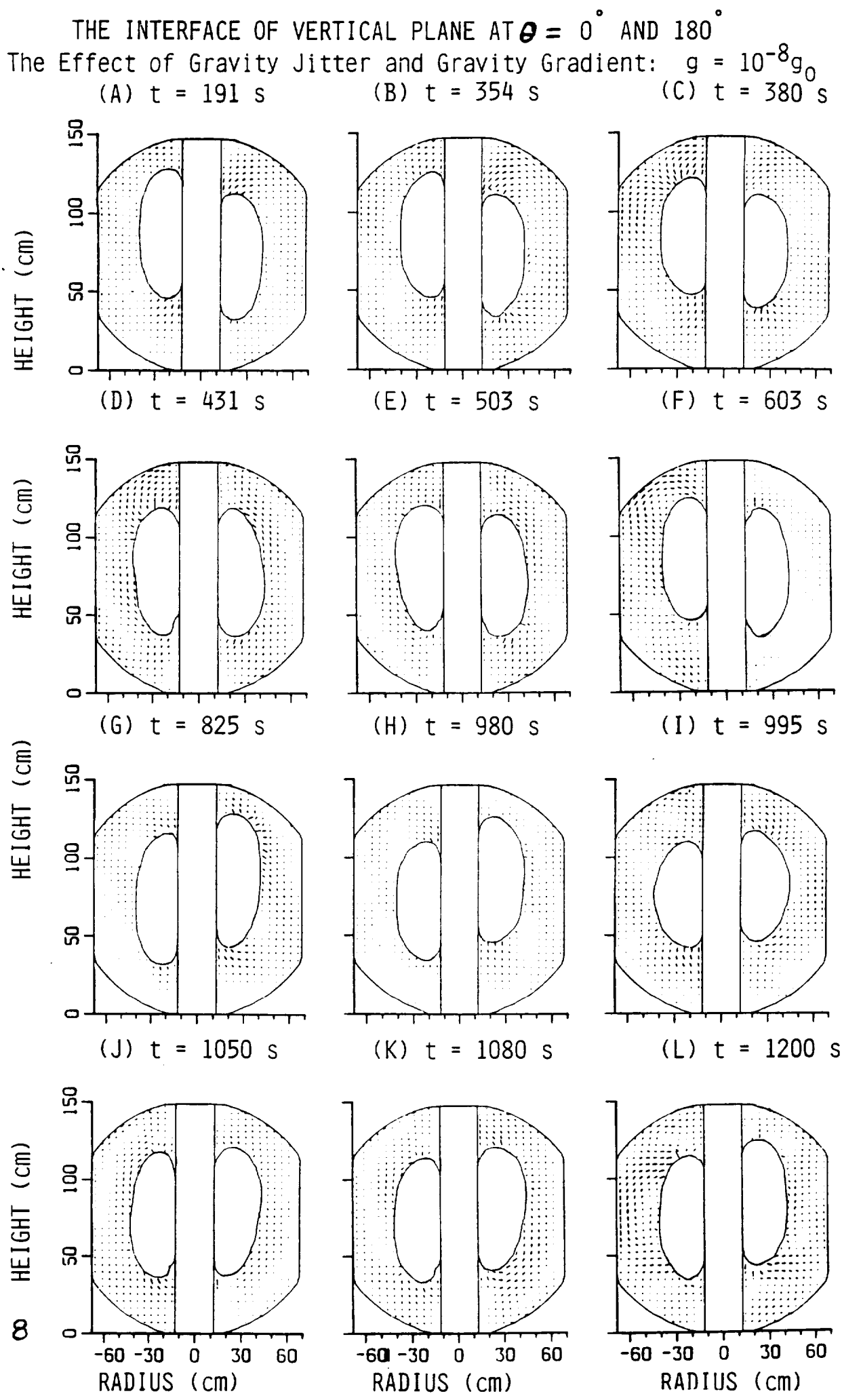
THE INTERFACE OF VERTICAL PLANE AT θ = 0° AND 180°
The Effect of Gravity Jitter and Gravity Gradient: g = 10^-8 g0
(A) t = 191 s
(B) t = 354 s
(C) t = 380 s
(D) t = 431 s
(E) t = 503 s
(F) t = 603 s
(G) t = 825 s
(H) t = 980 s
(I) t = 995 s
(J) t = 1050 s
(K) t = 1080 s
(L) t = 1200 s
HEIGHT (cm)
0
50
100
150
-60 -30 0 30 60
RADIUS (cm)

Fig. 8

THREE DIMENSIONAL LIQUID AND VAPOR INTERFACE

The Effect of Gravity Jitter and Gravity Gradient: $g = 10^{-6} g_0$

(A) t = 191 s

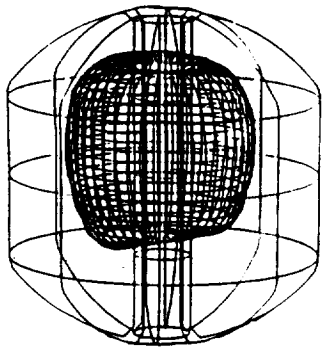

(B) t = 354 s

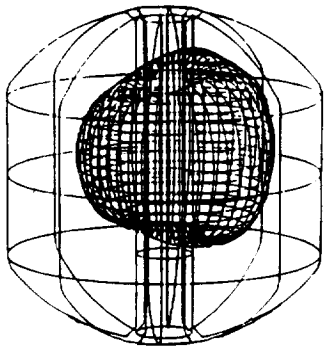

(C) t = 380 s

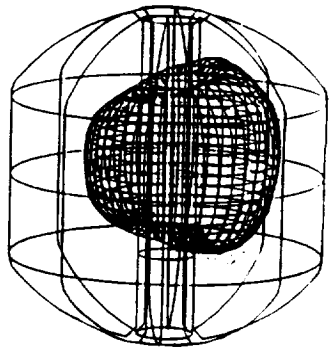

(D) t = 431 s

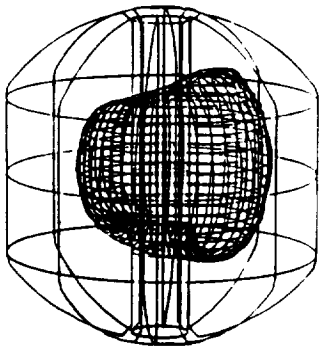

(E) t = 503 s

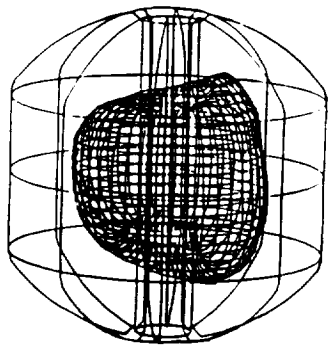

(F) t = 603 s

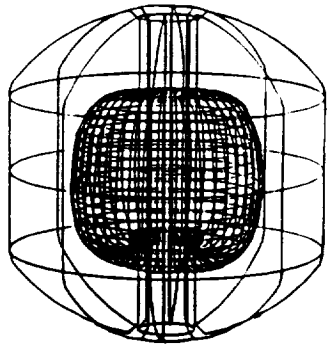

(G) t = 825 s

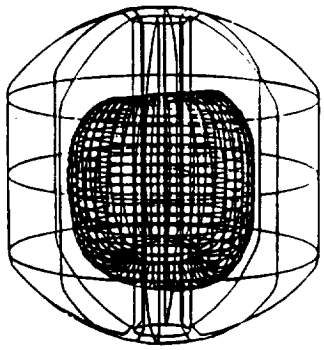

(H) t = 980 s

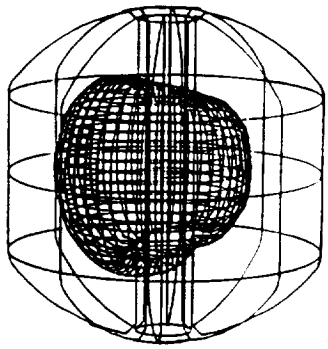

(I) t = 995 s

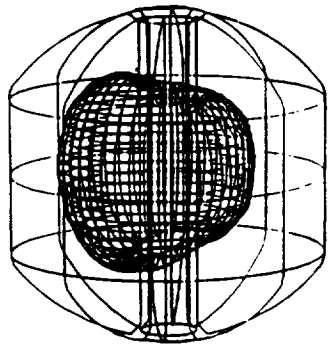

(J) t = 1050 s

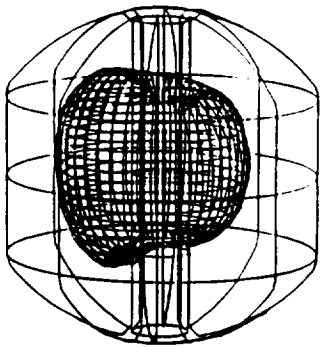

(K) t = 1080 s

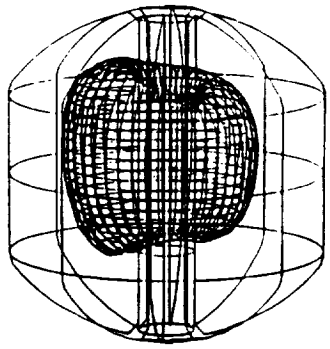

(L) t = 1200 s

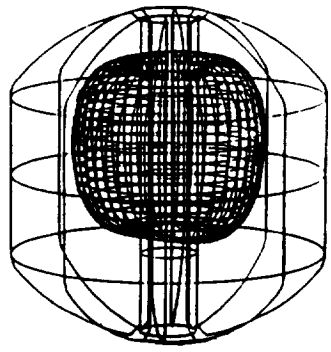

Fig. 9

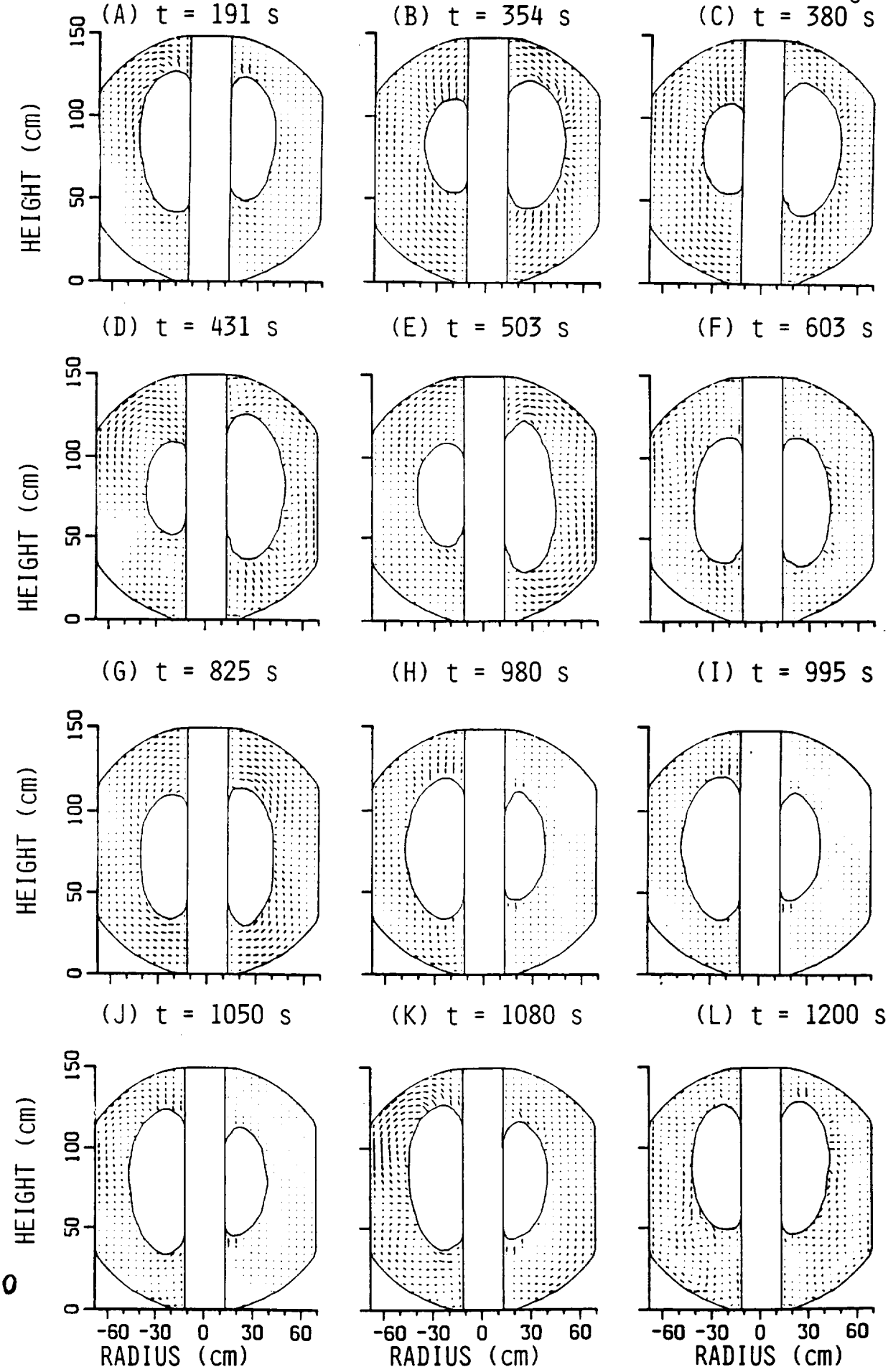
THE INTERFACE OF VERTICAL PLANE AT θ = 0° and 180°
The Effect of Gravity Jitter and Gravity Gradient: g = 10^-6 g0
(A) t = 191 s
(B) t = 354 s
(C) t = 380 s
(D) t = 431 s
(E) t = 503 s
(F) t = 603 s
(G) t = 825 s
(H) t = 980 s
(I) t = 995 s
(J) t = 1050 s
(K) t = 1080 s
(L) t = 1200 s
HEIGHT (cm)
0
50
100
150
-60 -30 0 30 60
RADIUS (cm)

Fig. 10

AXAF-S
Time Variation
of
Gravity Gradient
Acceleration
Associated With
Slew Motion

Acting on the
Fluid Mass Located
at

(r, θ, z)

$= (12\ cm, \pi/2, 3\ cm)$

$g_0 = 9.81\ m/s^2$

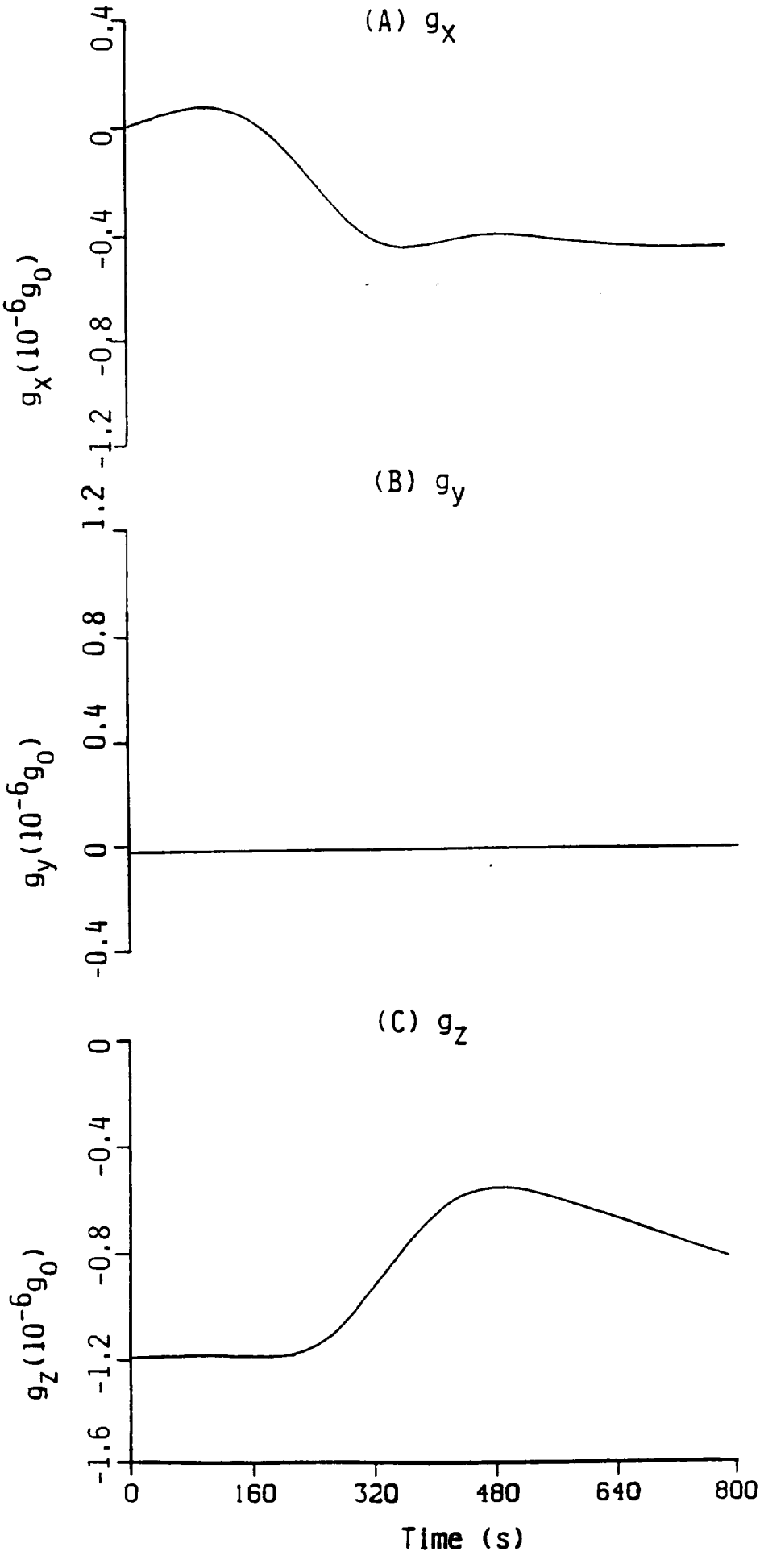

Fig. 11

INITIAL PROFILES OF LIQUID HELIUM AND VAPOR INTERFACE

AXAF Dewar, Liquid Filled Level = 70%

(A) r-z plane at θ = 0° and 180°

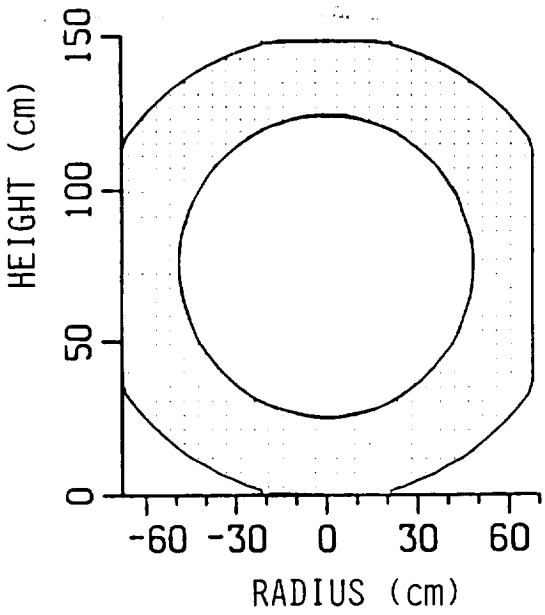

(B) r-z plane at θ = 90° and 180°

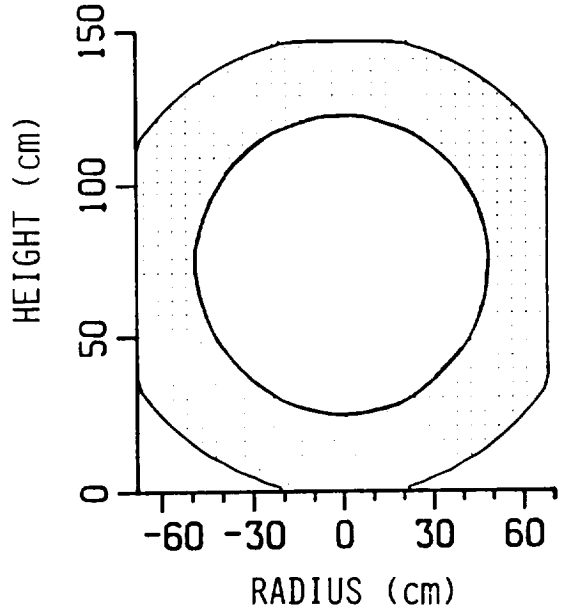

(C) r-θ plane at z = 95.9 cm

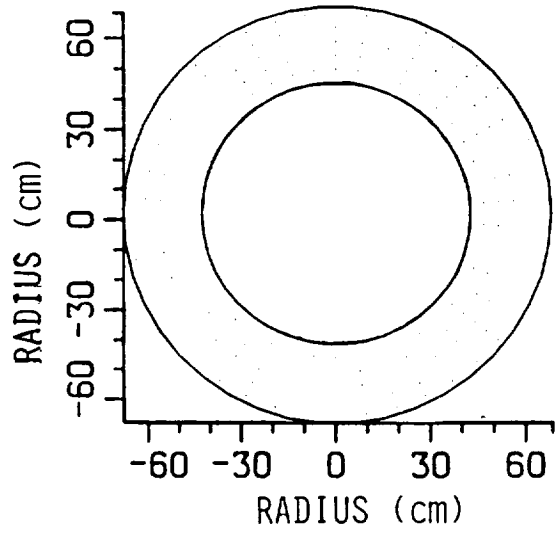

(D) Three Dimensional Profile

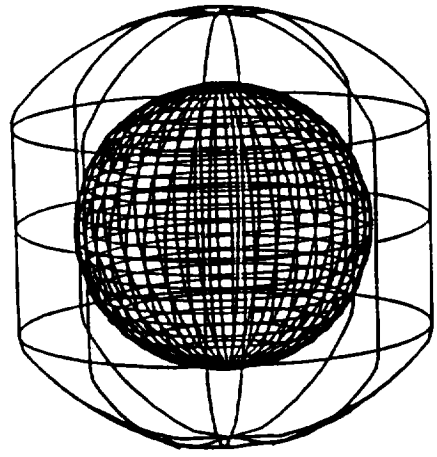

Fig. 12

SLOSHING DYNAMICS OF AXAF-S CRYOGENIC HELIUM II DEWAR
Driven by Gravity Gradient Acceleration, Liquid Filled Level = 70%

Three Dimensional Profiles

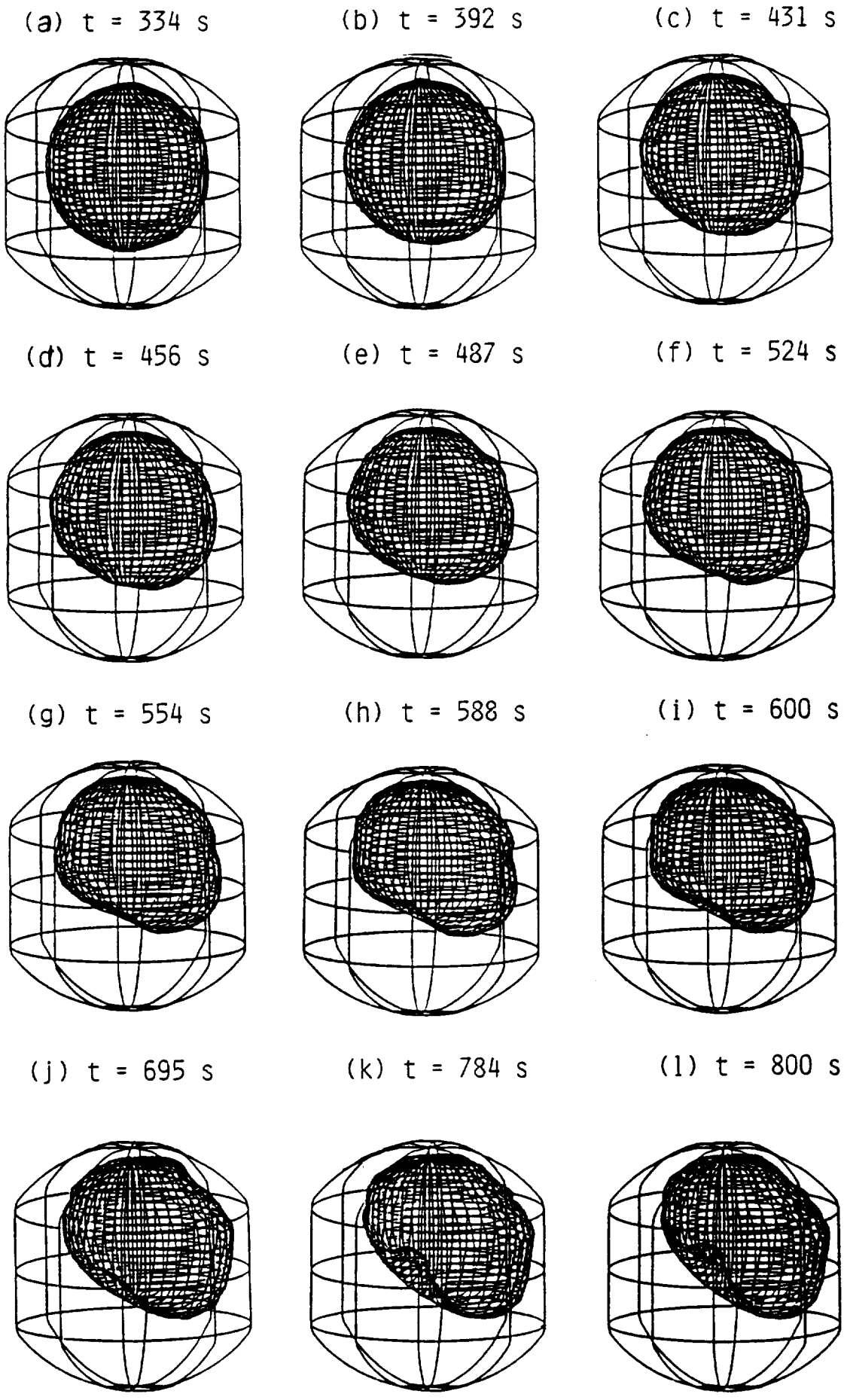

Fig. 13

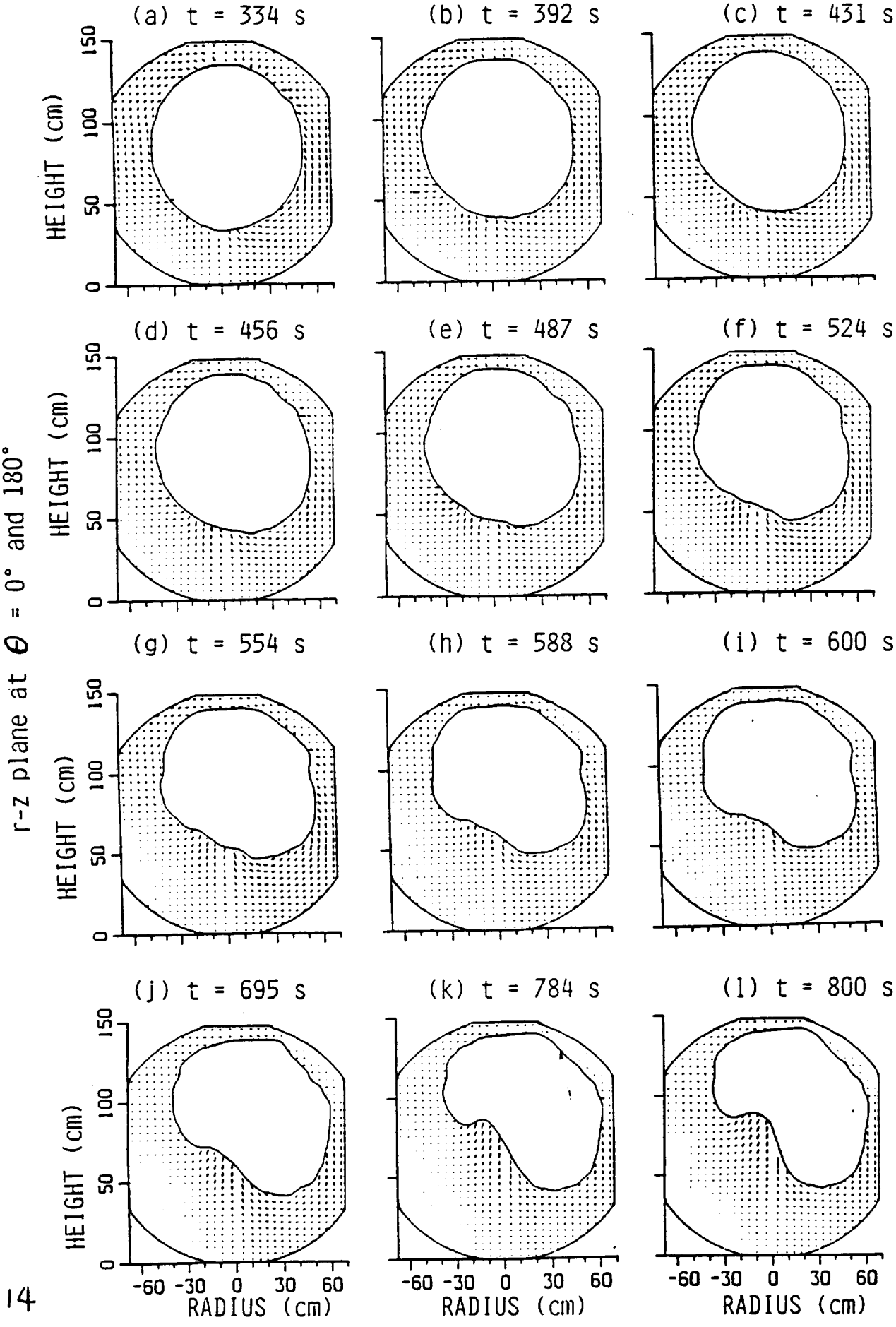
SLOSHING DYNAMICS OF AXAF-S CRYOGENIC HELIUM II DEWAR
Driven by Gravity Gradient Acceleration, Liquid Filled Level = 70%
(a) t = 334 s
(b) t = 392 s
(c) t = 431 s
(d) t = 456 s
(e) t = 487 s
(f) t = 524 s
(g) t = 554 s
(h) t = 588 s
(i) t = 600 s
(j) t = 695 s
(k) t = 784 s
(l) t = 800 s
HEIGHT (cm)
0
50
100
150
-60 -30 0 30 60
RADIUS (cm)
r-z plane at θ = 0° and 180°

Fig. 14